Nonequilibrium Fluctuation–Response Theory in the Frequency Domain

Euijoon Kwon,[1] Hyun-Myung Chun,[2] Hyunggyu Park,[1] and Jae Sung Lee[2,*]

[1]*Quantum Universe Center, Korea Institute for Advanced Study, Seoul 02455*

[2]*School of Physics, Korea Institute for Advanced Study, Seoul 02455, Republic of Korea*

(Dated: May 7, 2026)

We develop a unified fluctuation–response theory in the frequency domain for nonequilibrium steady states governed by overdamped Langevin dynamics and Markov jump processes. The relation expresses the power spectrum of general observables exactly as a quadratic form of local responses measured at the same frequency, thereby extending static nonequilibrium fluctuation–response relations to finite frequencies. The decomposition is spatial for Langevin systems and edge-resolved for Markov jump processes, and applies uniformly to state-dependent observables, current-like observables, and their combinations. As consequences of the same identity, we derive frequency-domain response uncertainty relations, kinetic and thermodynamic uncertainty relations, the equilibrium fluctuation–dissipation theorem, and Harada–Sasa-type relations. Applications to stochastic networks and driven diffusive systems illustrate how the theory resolves fluctuation spectra into edge-wise contributions and reveals frequency-dependent tradeoffs between fluctuations, response, and dissipation.

I. INTRODUCTION

Relating the response of a system to a weak perturbation to its spontaneous fluctuations is a central theme in statistical physics. At equilibrium, this connection is expressed by the fluctuation–dissipation theorem (FDT) [1]. Away from equilibrium, the direct equilibrium proportionality is generally lost, and several complementary routes have been developed to restore or quantify the fluctuation–response structure, including nonequilibrium FDTs [2–7] and Harada–Sasa-type relations connecting FDT violation to dissipation [8–10].

A closely related line of research has pursued universal constraints on fluctuations. Thermodynamic uncertainty relations (TURs) constrain current fluctuations by entropy production [11–15], while kinetic uncertainty relations (KURs) and thermodynamic–kinetic variants identify the complementary role of dynamical activity [16–21]. In contrast to FDT-type relations, which establish equalities linking fluctuations to response, these results take the form of inequalities that bound fluctuations. More recently, these ideas have been extended from fluctuation bounds to response bounds, showing that the sensitivity of nonequilibrium systems to kinetic and thermodynamic perturbations is itself constrained by fluctuations, dissipation, activity, and network topology [22–29].

The most recent development is the emergence of fluctuation–response relations (FRRs) far from equilibrium. For Markov jump processes, static FRRs were first derived to express long-time current covariances as quadratic combinations of local responses [30]. This structure was subsequently generalized to state observables and mixed state–current correlations [31, 32], while finite-time fluctuation–response inequalities extended the framework to broader classes of observables and dynamical responses [33]. In parallel, a time-domain FRR was recently derived for overdamped Langevin dynamics [34]. Frequency-domain formulations have also begun to appear, but so far mainly as inequalities [35], macroscopic Gaussian relations near stable fixed points [36], or finite-time relations for nonautonomous jump processes [37].

In this work, we derive an FRR in the frequency domain for nonequilibrium steady states of both overdamped Langevin systems and Markov jump processes. We show that the power spectrum of a broad class of observables, including state-dependent and current-like components, can be exactly reconstructed from local linear responses measured at the same frequency. The decomposition is spatial in the Langevin case, whereas for jump processes it is resolved at the level of edges. This frequency-domain FRR provides not only a finite-frequency extension of static nonequilibrium FRRs, but also an explicit decomposition of the power spectrum in terms of local responses.

The paper is organized as follows. In Sec. II we state the frequency-domain FRR and introduce the minimal notation. In Sec. III we derive the relation for overdamped Langevin systems, and in Sec. IV we develop the corresponding edge-resolved theory for Markov jump systems. In Sec. V we show how response uncertainty relations (RURs), response KUR and TUR, the equilibrium FDT, and Harada–Sasa-type relations follow from the same identity. In Sec. VI we illustrate the theory with examples of Markov jump networks and Langevin systems. More technical details are deferred to the appendices.

II. MAIN RESULTS

In this section, we state the central result of the paper: a unified FRR in the frequency domain for nonequilibrium steady states. The relation applies to both overdamped Langevin systems and Markov jump systems, and expresses the power spectrum of a broad class of ob-

* jslee@kias.re.kr

servables in terms of local linear responses to impulsive perturbations. As we explain below, this relation should be regarded as the foundational relation of the paper, since the frequency-domain RURs, TURs, the equilibrium FDT, and Harada–Sasa-type relations all arise from it as consequences.

A. Minimal definitions

We consider a system in a nonequilibrium steady state and an observable $A(t)$, or more generally a vector of observables $\boldsymbol{\theta}(t)$. In both the overdamped Langevin and Markov jump settings considered here, the observables of interest consist of two parts: a *state-dependent* part, which depends on the instantaneous state of the system, and a *current-like* part, which depends on the instantaneous dynamical increments. The precise forms of these observables will be specified in Secs. III and IV.

To characterize fluctuations, we introduce the covariance notation

$$C_{A,B}(\omega) = \int_{-\infty}^{\infty} \Big[\langle A(t)B(0)\rangle - \langle A\rangle_{\rm ss}\langle B\rangle_{\rm ss}\Big] e^{i\omega t}\, dt, \quad (1)$$

where $A(t)$ and $B(t)$ may be scalar- or vector-valued stochastic processes, provided that the product $A(t)B(0)$ is well-defined. In particular, for a vector observable $\boldsymbol{\theta}(t)$, the power spectrum matrix is denoted by $C_{\boldsymbol{\theta},\boldsymbol{\theta}^{\mathsf{T}}}(\omega)$.

To characterize responses, we consider local impulsive perturbations of a dynamical quantity $\phi_k(\boldsymbol{x})$, where $\boldsymbol{x}$ denotes the state of the system. The index k labels spatial components in the Langevin case and edges in the Markov jump case. In the Langevin setting, ϕ represents one of $\boldsymbol{F}$ (force), $\ln M$ (log-mobility), or T (temperature), while in the Markov jump case it represents either the symmetric or antisymmetric part of a transition rate. For an impulsive perturbation applied at time $t = 0$, we define the local frequency-domain response of an observable $A(t)$ as

$$R^{A}_{\phi_k(\boldsymbol{x})}(\omega) = \int_{0}^{\infty} \frac{\delta\langle A(t)\rangle}{\delta\phi_k(\boldsymbol{x},0)} e^{i\omega t}\, dt, \quad (2)$$

where the second argument of $\phi_k(\boldsymbol{x}, 0)$ in the functional derivative specifies the time at which the perturbation is applied.

We also introduce notation for responses to global perturbations. For a force perturbation of the form $\boldsymbol{F}(\boldsymbol{x}) \mapsto \boldsymbol{F}(\boldsymbol{x}) + \epsilon\boldsymbol{\psi}(\boldsymbol{x})$, the corresponding response of an observable A is denoted by $R^{A}_{\boldsymbol{F}\mapsto\boldsymbol{F}+\epsilon\boldsymbol{\psi}}(\omega)$ and can be expressed in terms of the local responses as

$$R^{A}_{\boldsymbol{F}\mapsto\boldsymbol{F}+\epsilon\boldsymbol{\psi}}(\omega) = \sum_k \int d\boldsymbol{x}\, \psi_k(\boldsymbol{x})\, R^{A}_{F_k(\boldsymbol{x})}(\omega). \quad (3)$$

Analogous expressions hold for global perturbations of $\ln M$ and T in the Langevin setting, and for the corresponding global perturbations of transition rates in the Markov jump case.

B. Frequency-domain fluctuation–response relation

We now state the main result of the paper. This result has two realizations, one for overdamped Langevin dynamics and one for Markov jump dynamics, but the structure is the same in both cases: the fluctuation spectrum of an observable can be reconstructed from local linear responses measured at the same frequency.

For overdamped Langevin systems, the frequency-domain FRR takes the form

$$C_{\boldsymbol{\theta},\boldsymbol{\theta}^{\mathsf{T}}}(\omega) = \sum_{k,l=1}^{N} \int d\boldsymbol{z}\, R^{\boldsymbol{\theta}}_{\phi_k(\boldsymbol{z})}(\omega) \left[A^{\phi}(\boldsymbol{z})^{-1}\right]_{kl} \left[R^{\boldsymbol{\theta}}_{\phi_l(\boldsymbol{z})}(\omega)\right]^{\dagger}, \quad (4)$$

where $\phi \in \{\boldsymbol{F}, \ln M, T\}$, and $A^{\phi}(\boldsymbol{z})$ is a positive matrix determined by the steady state and the type of perturbation. The superscript $\dagger$ denotes Hermitian conjugate of vectors and matrices. Its explicit form is given in Sec. III.

For Markov jump systems, the corresponding relation is

$$C_{\boldsymbol{\theta},\boldsymbol{\theta}^{\mathsf{T}}}(\omega) = \sum_{n>m} \frac{1}{A^{\phi}_{nm}} R^{\boldsymbol{\theta}}_{\phi_{nm}}(\omega) \left[R^{\boldsymbol{\theta}}_{\phi_{nm}}(\omega)\right]^{\dagger}, \quad (5)$$

where $\phi \in \{B, F\}$, the label ϕ_{nm} refers to a local perturbation associated with the edge $m \leftrightarrow n$, and A^{ϕ}_{nm} is a positive scalar weight determined by the steady state and by the type of perturbation. Its explicit form is given in Sec. IV.

Equations (4) and (5) constitute the central results of this work. In both continuous and discrete dynamics, they express the power spectrum as a quadratic form of local responses. The decomposition is spatial for Langevin systems and edge-resolved for Markov jump processes. This representation makes explicit how local response contributions at different spatial locations or edges enter the spectrum.

C. Interpretation and significance

The relations (4) and (5) are finite-frequency fluctuation–response identities for nonequilibrium steady states. Unlike inequalities relating fluctuations and response, they establish an explicit equality expressing the power spectrum at finite frequency as a quadratic combination of local linear responses. Thus, the frequency-domain FRR provides a unified framework for relating spontaneous fluctuations to controlled perturbations far from equilibrium.

This result is structurally different from the equilibrium FDT. In equilibrium, fluctuations and responses are related by a direct proportionality [1]. Out of equilibrium, such a simple proportionality is generally lost. This loss, however, does not imply the absence of structure.

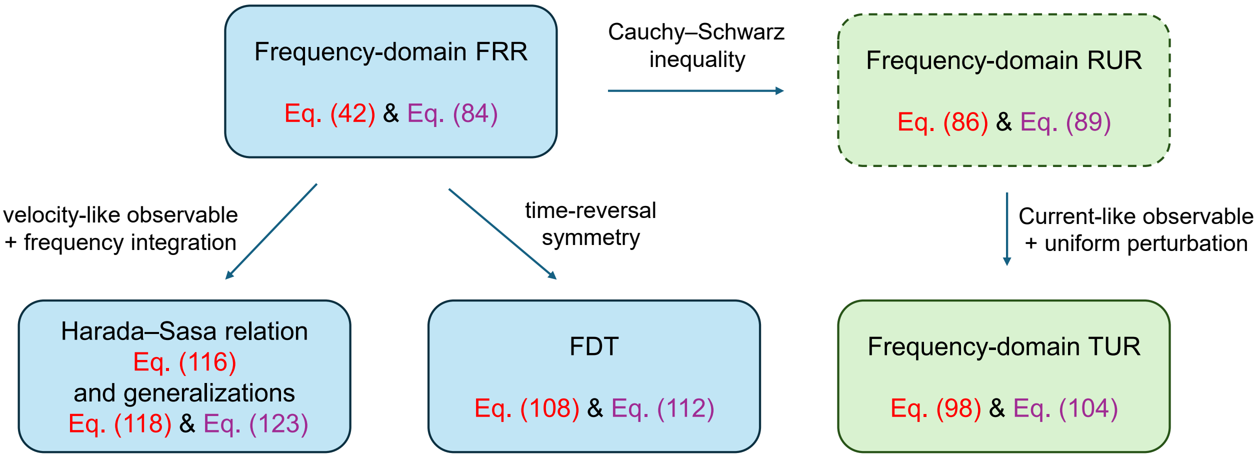

FIG. 1. A hierarchy of the relations derived in this work. The frequency-domain FRR sits at the top of the hierarchy as the foundational relation. Blue boxes denote exact equalities, while green boxes represent inequalities. Each arrow indicates how a lower-level relation is obtained from a higher-level one. Equation numbers are colored in red for overdamped Langevin systems and in purple for Markov jump processes. The dotted box indicates a relation that reduces to previously reported results in appropriate limits (Refs. [35, 36]).

Rather, the power spectrum remains exactly expressible as a weighted quadratic combination of local responses.

It is important to position the present result relative to recent literature. Nonequilibrium FRRs were first established for Markov jump processes in the static, long-time limit, initially for current observables [30], and then extended to state observables and mixed state–current covariances [31, 32]. In parallel, a time-domain fluctuation–response theory has been developed for overdamped Langevin dynamics, which unifies long-time FRRs, finite-time fluctuation–response inequalities, and response uncertainty relations within a single hierarchical structure [34]. More recently, extensions to the frequency domain have also been developed, but in the form of a finite-frequency inequality [35] or in a macroscopic Gaussian theory valid near stable fixed points [36]. Such approaches either constrain the response relative to the spectrum without reconstructing it, or are valid only within a regime of weak fluctuations around stable deterministic states. Against this background, the present result fills an important gap: it establishes a finite-frequency FRR that reconstructs the power spectrum through an equality at finite frequency without relying on a Gaussian approximation. Finally, a finite-time fluctuation–response theory for nonautonomous jump processes developed in [37] expresses covariance (the frequency-integrated power spectrum) in terms of Fourier components of response functions. While it does not provide a frequency-resolved reconstruction of the power spectrum, it provides a complementary extension of fluctuation–response relations to nonstationary dynamics by lifting the steady-state restriction.

A further strength of the present result is its breadth across observables. The same structure applies to current-like observables, state-dependent observables, and their combinations. This is natural in settings where both occupations and transport are described within a common formalism. It also enables a direct interpretation of the power spectrum, by distinguishing contributions from local residence statistics, transport channels, and their interplay.

Finally, the significance of the frequency-domain FRR lies in the results it generates. Once the exact identity is established, the frequency-domain RUR and related inequalities arise from applications of the Cauchy–Schwarz inequality; KUR and TUR arise from specific perturbations; the equilibrium limit recovers the FDT; and the nonequilibrium remainder yields Harada–Sasa-type dissipation relations [8–10]. For this reason, the frequency-domain FRR should be regarded as the foundational relation of this work. The hierarchy stemming from the frequency-domain FRR is illustrated in Fig. 1.

III. FLUCTUATION–RESPONSE THEORY IN OVERDAMPED LANGEVIN SYSTEMS

In this section, we construct the frequency-domain FRR for overdamped Langevin systems. We begin by specifying the stochastic dynamics and the perturbations of interest, and then introduce the class of observables together with the empirical density and current fields. The central object of the construction is a frequency-domain excess propagator that determines both local responses and two-point covariances. Since both quantities can be expressed in terms of this excess propagator, this structure leads first to a local FRR for empirical density and current, and then, by linearity, to the FRR for general observables. Technical derivations are deferred to Appendix A.

A. Setup and notation

Throughout this section, $\boldsymbol{x}, \boldsymbol{y}, \boldsymbol{z} \in \mathbb{R}^N$ denote configuration vectors. We consider an N-dimensional overdamped Langevin system governed by

$$\dot{\boldsymbol{x}}(t) = M(\boldsymbol{x}(t))\boldsymbol{F}(\boldsymbol{x}(t)) + \sqrt{2}\,B(\boldsymbol{x}(t)) \circledast \boldsymbol{\xi}(t), \tag{6}$$

where $\circledast$ denotes the anti-Itô product, $\boldsymbol{F}(\boldsymbol{x})$ is the drift force, $M(\boldsymbol{x})$ is the mobility matrix, $B(\boldsymbol{x})$ is the noise-amplitude matrix, and $\boldsymbol{\xi}(t)$ is Gaussian white noise with

$$\langle \boldsymbol{\xi}(t) \rangle = \boldsymbol{0}, \qquad \langle \xi_i(t)\xi_j(t') \rangle = \delta_{ij}\delta(t-t'). \tag{7}$$

Equivalently, the same dynamics can be written in Itô form as

$$\dot{\boldsymbol{x}}(t) = \boldsymbol{v}(\boldsymbol{x}(t)) + \sqrt{2}\,B(\boldsymbol{x}(t)) \bullet \boldsymbol{\xi}(t), \tag{8}$$

where $\bullet$ is the Itô product and $\boldsymbol{v}$ is the effective drift defined as

$$\boldsymbol{v}(\boldsymbol{x}) = M(\boldsymbol{x})\boldsymbol{F}(\boldsymbol{x}) + \left[\boldsymbol{\nabla}_{\boldsymbol{x}}^{\mathsf{T}} D(\boldsymbol{x})\right]^{\mathsf{T}}, \tag{9}$$

where $\boldsymbol{\nabla}_{\boldsymbol{x}} \equiv (\partial_{x_1}, \cdots, \partial_{x_N})^{\mathsf{T}}$ is the gradient operator written as a column vector and $D(\boldsymbol{x}) = \frac{1}{2}B(\boldsymbol{x})B(\boldsymbol{x})^{\mathsf{T}}$. The superscript T denotes transposition of vectors and matrices.

For notational simplicity, we assume $M(\boldsymbol{x})$ and $D(\boldsymbol{x})$ are diagonal,

$$\begin{aligned} M(\boldsymbol{x}) &= \mathrm{diag}\big(\mu_1(\boldsymbol{x}), \ldots, \mu_N(\boldsymbol{x})\big), \\ D(\boldsymbol{x}) &= \mathrm{diag}\big(D_1(\boldsymbol{x}), \ldots, D_N(\boldsymbol{x})\big), \end{aligned} \tag{10}$$

and define the temperature matrix by

$$T(\boldsymbol{x}) = \mathrm{diag}\big(T_1(\boldsymbol{x}), \ldots, T_N(\boldsymbol{x})\big), \tag{11}$$

such that

$$D(\boldsymbol{x}) = M(\boldsymbol{x})T(\boldsymbol{x}) = T(\boldsymbol{x})M(\boldsymbol{x}). \tag{12}$$

We further assume that the dynamics admits a unique nonequilibrium steady state with probability density $\pi(\boldsymbol{x})$. The corresponding steady-state probability current is denoted by $\boldsymbol{j}_{\mathrm{ss}}(\boldsymbol{x})$. The theory can be readily extended to non-diagonal matrices.

We consider the response to small perturbations and their relation to steady-state fluctuations. To treat them on equal footing, we denote the perturbed quantity by ϕ, with $\phi \in \{\boldsymbol{F}, \ln M, T\}$. A local impulsive perturbation of the kth component of ϕ is written as

$$\phi_k(\boldsymbol{x}) \mapsto \phi_k(\boldsymbol{x}) + \epsilon\,\delta(\boldsymbol{x}-\boldsymbol{z})\delta(t-s), \tag{13}$$

where ϵ is infinitesimal. Local perturbations are the elementary building blocks of the FRR. Global perturbations are defined in (3) and used later when discussing RURs and related consequences. Perturbations of the mobility induce no response at equilibrium and therefore probe nonequilibrium features, since they modify only the characteristic time scale of the dynamics [23, 27, 33, 34]. They are not reducible to conventional force perturbations.

B. Observables, empirical fields, and response functions

We introduce the observables and local fields entering the FRR. A general observable consists of a state-dependent part and a current-like part. For a single observable, we write

$$\theta(t) = \Lambda(\boldsymbol{x}(t))^{\mathsf{T}} \circ \dot{\boldsymbol{x}}(t) + g(\boldsymbol{x}(t)), \tag{14}$$

where the first term is current-like and the second term is state-dependent. The product $\circ$ denotes the Stratonovich product. More generally, for a collection of N_O observables we write

$$\boldsymbol{\theta}(t) = L(\boldsymbol{x}(t)) \circ \dot{\boldsymbol{x}}(t) + G(\boldsymbol{x}(t)). \tag{15}$$

Here, $L(\boldsymbol{x})$ is an $N_O \times N$ matrix-valued function and $G(\boldsymbol{x})$ is an N_O-dimensional vector-valued function. This form includes purely state-dependent observables, purely current-like observables, and their combinations.

The local objects underlying (15) are the empirical density and empirical current,

$$\rho(\boldsymbol{x},t) \equiv \delta(\boldsymbol{x}-\boldsymbol{x}(t)), \qquad \boldsymbol{\jmath}(\boldsymbol{x},t) \equiv \delta(\boldsymbol{x}-\boldsymbol{x}(t)) \circ \dot{\boldsymbol{x}}(t). \tag{16}$$

In terms of these fields, the observable vector reads

$$\boldsymbol{\theta}(t) = \int d\boldsymbol{x}\,\Big[G(\boldsymbol{x})\rho(\boldsymbol{x},t) + L(\boldsymbol{x})\boldsymbol{\jmath}(\boldsymbol{x},t)\Big]. \tag{17}$$

Thus, the fluctuations and responses of $\boldsymbol{\theta}(t)$ follow from those of $\rho(\boldsymbol{x},t)$ and $\boldsymbol{\jmath}(\boldsymbol{x},t)$ by integration with the weights G and L.

Using the notation in (1), we write the empirical-field covariances as $C_{\rho(\boldsymbol{x}),\rho(\boldsymbol{y})}(\omega)$, $C_{\rho(\boldsymbol{x}),\boldsymbol{\jmath}(\boldsymbol{y})^{\mathsf{T}}}(\omega)$, and $C_{\boldsymbol{\jmath}(\boldsymbol{x}),\boldsymbol{\jmath}(\boldsymbol{y})^{\mathsf{T}}}(\omega)$, and the observable-level power spectrum as $C_{\boldsymbol{\theta},\boldsymbol{\theta}^{\mathsf{T}}}(\omega)$. Similarly, using the response notation in (2), we write the corresponding local responses as $R^{\rho(\boldsymbol{x})}_{\phi_k(\boldsymbol{z})}(\omega)$, $R^{\boldsymbol{\jmath}(\boldsymbol{x})}_{\phi_k(\boldsymbol{z})}(\omega)$, and $R^{\boldsymbol{\theta}}_{\phi_k(\boldsymbol{z})}(\omega)$. The next two subsections show that the local covariance functions of the empirical fields can be written as quadratic forms of the corresponding local responses.

C. Excess propagator and local responses

The central object in the frequency-domain response theory for overdamped Langevin systems is an excess propagator. It encodes how the responses of the empirical density and current, induced by impulsive perturbations, propagate through the unperturbed steady-state dynamics.

We denote by $P(\boldsymbol{x},t|\boldsymbol{y},s)$ the transition probability density of the unperturbed dynamics. It satisfies the Fokker–Planck equation

$$\partial_t P(\boldsymbol{x},t|\boldsymbol{y},s) = \hat{\mathcal{L}}_{\boldsymbol{x}} P(\boldsymbol{x},t|\boldsymbol{y},s), \tag{18}$$

where $\hat{\mathcal{L}}_{\boldsymbol{x}}$ is the Fokker–Planck generator acting on the variable $\boldsymbol{x}$. We write

$$\hat{\mathcal{L}}_{\boldsymbol{x}} = -\nabla_{\boldsymbol{x}}^{\mathsf{T}} \hat{\mathcal{J}}_{\boldsymbol{x}}, \qquad \hat{\mathcal{J}}_{\boldsymbol{x}} = M(\boldsymbol{x})\big[\boldsymbol{F}(\boldsymbol{x}) - T(\boldsymbol{x})\nabla_{\boldsymbol{x}}\big]. \tag{19}$$

The steady-state density is characterized by

$$\hat{\mathcal{L}}_{\boldsymbol{x}}\pi(\boldsymbol{x}) = 0. \tag{20}$$

The corresponding steady-state current is

$$\boldsymbol{j}_{\rm ss}(\boldsymbol{x}) = \hat{\mathcal{J}}_{\boldsymbol{x}}\pi(\boldsymbol{x}). \tag{21}$$

The excess propagator is defined by [38]

$$H(\boldsymbol{x},\boldsymbol{z};\omega) = \int_0^\infty \big[P(\boldsymbol{x},t|\boldsymbol{z},0) - \pi(\boldsymbol{x})\big] e^{i\omega t}\, dt. \tag{22}$$

It measures the excess probability at $\boldsymbol{x}$ relative to the steady state, following a localized initial condition at $\boldsymbol{z}$, at frequency ω.

The excess propagator satisfies the identities

$$\int d\boldsymbol{z}\, H(\boldsymbol{x},\boldsymbol{z};\omega)\pi(\boldsymbol{z}) = 0, \tag{23}$$

$$\big(i\omega + \hat{\mathcal{L}}_{\boldsymbol{x}}\big) H(\boldsymbol{x},\boldsymbol{z};\omega) = -\delta(\boldsymbol{x}-\boldsymbol{z}) + \pi(\boldsymbol{x}), \tag{24}$$

and

$$\big(i\omega + \hat{\mathcal{L}}_{\boldsymbol{z}}^{\dagger}\big) H(\boldsymbol{x},\boldsymbol{z};\omega) = -\delta(\boldsymbol{x}-\boldsymbol{z}) + \pi(\boldsymbol{x}). \tag{25}$$

These relations show that H plays the role of the steady-state projected resolvent of the Fokker–Planck dynamics. Their derivations are provided in Appendix. A 2.

We consider a local impulsive perturbation of $\phi_k(\boldsymbol{z})$ as in (13). At the level of the Fokker–Planck generator, this perturbation reads

$$\hat{\mathcal{L}}_{\boldsymbol{x}} \mapsto \hat{\mathcal{L}}_{\boldsymbol{x}} - \epsilon\delta(t)\, \nabla_{\boldsymbol{x}}^{\mathsf{T}}\delta(\boldsymbol{x}-\boldsymbol{z})\, \hat{\mathcal{K}}_{\phi_k,\boldsymbol{x}}\,, \tag{26}$$

where the operator $\hat{\mathcal{K}}_{\phi_k,\boldsymbol{x}}$ depends on the choice of the perturbed quantity (see Eqs. (A7)–(A9)). We define the associated local prefactor by

$$N_{\phi_k}(\boldsymbol{z}) \equiv \hat{\mathcal{K}}_{\phi_k,\boldsymbol{z}}\pi(\boldsymbol{z}). \tag{27}$$

Its explicit form depends on whether ϕ corresponds to the force, mobility, or temperature (see Eqs. (A20)–(A22)), but the local response structure is identical in all cases.

The local response of the empirical density reads

$$R^{\rho(\boldsymbol{x})}_{\phi_k(\boldsymbol{z})}(\omega) = \big[N_{\phi_k}(\boldsymbol{z})\big]^{\mathsf{T}} \nabla_{\boldsymbol{z}} H(\boldsymbol{x},\boldsymbol{z};\omega). \tag{28}$$

Similarly, the local response of the empirical current reads

$$R^{\boldsymbol{\jmath}(\boldsymbol{x})}_{\phi_k(\boldsymbol{z})}(\omega) = \mathcal{P}(\boldsymbol{x},\boldsymbol{z};\omega)\, N_{\phi_k}(\boldsymbol{z}), \tag{29}$$

where

$$\mathcal{P}(\boldsymbol{x},\boldsymbol{z};\omega) = I\,\delta(\boldsymbol{x}-\boldsymbol{z}) + \hat{\mathcal{J}}_{\boldsymbol{x}}\nabla_{\boldsymbol{z}}^{\mathsf{T}} H(\boldsymbol{x},\boldsymbol{z};\omega). \tag{30}$$

with I denoting the $N\times N$ identity matrix. Equations (28) and (29) show that both density and current responses are determined by the same excess propagator. The perturbation type enters only through the local prefactor $N_{\phi_k}(\boldsymbol{z})$. The derivations of (28) and (29) are given in Appendix A 1.

D. Local fluctuation–response relation for empirical density and current

We show that the local covariance functions of the empirical density and current are determined by the same excess propagator that governs the local responses in Sec. III C. This establishes the local form of the frequency-domain FRR.

A direct calculation of the steady-state two-time distribution gives

$$C_{\rho(\boldsymbol{x}),\rho(\boldsymbol{y})}(\omega) = H(\boldsymbol{x},\boldsymbol{y};\omega)\pi(\boldsymbol{y}) + H(\boldsymbol{y},\boldsymbol{x};-\omega)\pi(\boldsymbol{x}). \tag{31}$$

The key step is the identity that rewrites the right-hand side of (31) as a quadratic form in $\nabla_{\boldsymbol{z}} H$:

$$\begin{aligned} &C_{\rho(\boldsymbol{x}),\rho(\boldsymbol{y})}(\omega) \\ &= 2\int d\boldsymbol{z}\, \pi(\boldsymbol{z})\, \nabla_{\boldsymbol{z}}^{\mathsf{T}} H(\boldsymbol{x},\boldsymbol{z};\omega)\, D(\boldsymbol{z})\, \nabla_{\boldsymbol{z}} H(\boldsymbol{y},\boldsymbol{z};-\omega). \end{aligned} \tag{32}$$

The proof of (32) is deferred to Appendix A 4.

Using (30), the mixed and current–current covariances can be written in parallel form

$$\begin{aligned} &C_{\rho(\boldsymbol{x}),\boldsymbol{\jmath}(\boldsymbol{y})^{\mathsf{T}}}(\omega) \\ &= 2\int d\boldsymbol{z}\, \pi(\boldsymbol{z})\, \nabla_{\boldsymbol{z}}^{\mathsf{T}} H(\boldsymbol{x},\boldsymbol{z};\omega)\, D(\boldsymbol{z})\, \big[\mathcal{P}(\boldsymbol{y},\boldsymbol{z};\omega)\big]^{\dagger}, \end{aligned} \tag{33}$$

and

$$C_{\boldsymbol{\jmath}(\boldsymbol{x}),\boldsymbol{\jmath}(\boldsymbol{y})^{\mathsf{T}}}(\omega) = 2\int d\boldsymbol{z}\,\pi(\boldsymbol{z})\,\mathcal{P}(\boldsymbol{x},\boldsymbol{z};\omega)\,D(\boldsymbol{z})\,\left[\mathcal{P}(\boldsymbol{y},\boldsymbol{z};\omega)\right]^{\dagger}. \tag{34}$$

Equations (32)–(34) make clear that the local covariance functions are built from the same objects that appear in the response formulas (28) and (29). The proofs of (33) and (34) are deferred to Appendix A 3.

To make this connection explicit, we define the matrix of local prefactors

$$N^{\phi}(\boldsymbol{z}) = \big(N_{\phi_1}(\boldsymbol{z}),\ldots,N_{\phi_N}(\boldsymbol{z})\big)^{\mathsf{T}}, \tag{35}$$

and the associated perturbation weight matrix

$$A^{\phi}(\boldsymbol{z}) = \frac{1}{2\pi(\boldsymbol{z})}\left[N^{\phi}(\boldsymbol{z})\right]^{\mathsf{T}} D(\boldsymbol{z})^{-1} N^{\phi}(\boldsymbol{z}). \tag{36}$$

The explicit forms of the matrices $A^{\phi}(\boldsymbol{z})$ for $\phi \in \{\boldsymbol{F},\ln M,T\}$ are given in Appendix A 5. Combining (28) with (32) yields

$$C_{\rho(\boldsymbol{x}),\rho(\boldsymbol{y})}(\omega) = \sum_{k,l=1}^{N}\int d\boldsymbol{z}\,R^{\rho(\boldsymbol{x})}_{\phi_k(\boldsymbol{z})}(\omega)\,\left[A^{\phi}(\boldsymbol{z})^{-1}\right]_{kl}\,R^{\rho(\boldsymbol{y})}_{\phi_l(\boldsymbol{z})}(-\omega). \tag{37}$$

Likewise, combining (28) and (29) with (33) and (34), we obtain

$$C_{\rho(\boldsymbol{x}),\boldsymbol{\jmath}(\boldsymbol{y})^{\mathsf{T}}}(\omega) = \sum_{k,l=1}^{N}\int d\boldsymbol{z}\,R^{\rho(\boldsymbol{x})}_{\phi_k(\boldsymbol{z})}(\omega)\,\left[A^{\phi}(\boldsymbol{z})^{-1}\right]_{kl}\,\left[R^{\boldsymbol{\jmath}(\boldsymbol{y})}_{\phi_l(\boldsymbol{z})}(\omega)\right]^{\dagger}, \tag{38}$$

and

$$C_{\boldsymbol{\jmath}(\boldsymbol{x}),\boldsymbol{\jmath}(\boldsymbol{y})^{\mathsf{T}}}(\omega) = \sum_{k,l=1}^{N}\int d\boldsymbol{z}\,R^{\boldsymbol{\jmath}(\boldsymbol{x})}_{\phi_k(\boldsymbol{z})}(\omega)\,\left[A^{\phi}(\boldsymbol{z})^{-1}\right]_{kl}\,\left[R^{\boldsymbol{\jmath}(\boldsymbol{y})}_{\phi_l(\boldsymbol{z})}(\omega)\right]^{\dagger}. \tag{39}$$

Equations (37)–(39) constitute the local frequency-domain FRR for overdamped Langevin systems. They show that the local covariance functions of empirical density and current are given by integrals of products of local responses over the perturbation point $\boldsymbol{z}$, weighted by the inverse of the matrix $A^{\phi}(\boldsymbol{z})$.

E. Frequency-domain fluctuation–response relation for general observables

Given the local relations (37)–(39), the extension to general observables is immediate. Since the observable vector $\boldsymbol{\theta}$ in (17) is linear in the empirical density and current, the local response is given by

$$R^{\boldsymbol{\theta}}_{\phi_k(\boldsymbol{z})}(\omega) = \int d\boldsymbol{x}\,\Big[G(\boldsymbol{x})\,R^{\rho(\boldsymbol{x})}_{\phi_k(\boldsymbol{z})}(\omega) + L(\boldsymbol{x})\,R^{\boldsymbol{\jmath}(\boldsymbol{x})}_{\phi_k(\boldsymbol{z})}(\omega)\Big]. \tag{40}$$

Similarly, the power spectrum matrix of $\boldsymbol{\theta}(t)$ reads

$$\begin{aligned} C_{\boldsymbol{\theta},\boldsymbol{\theta}^{\mathsf{T}}}(\omega) = \int d\boldsymbol{x}\,d\boldsymbol{y}\,\Big[&G(\boldsymbol{x})\,C_{\rho(\boldsymbol{x}),\rho(\boldsymbol{y})}(\omega)\,G(\boldsymbol{y})^{\mathsf{T}} \\ &+ G(\boldsymbol{x})\,C_{\rho(\boldsymbol{x}),\boldsymbol{\jmath}(\boldsymbol{y})^{\mathsf{T}}}(\omega)\,L(\boldsymbol{y})^{\mathsf{T}} \\ &+ L(\boldsymbol{x})\,C_{\boldsymbol{\jmath}(\boldsymbol{x}),\rho(\boldsymbol{y})}(\omega)\,G(\boldsymbol{y})^{\mathsf{T}} \\ &+ L(\boldsymbol{x})\,C_{\boldsymbol{\jmath}(\boldsymbol{x}),\boldsymbol{\jmath}(\boldsymbol{y})^{\mathsf{T}}}(\omega)\,L(\boldsymbol{y})^{\mathsf{T}}\Big]. \end{aligned} \tag{41}$$

Substituting (37)–(39) into (41) and using (40), the integrations over $\boldsymbol{x}$ and $\boldsymbol{y}$ combine into the local responses of the observable $\boldsymbol{\theta}$. One obtains

$$C_{\boldsymbol{\theta},\boldsymbol{\theta}^{\mathsf{T}}}(\omega) = \sum_{k,l=1}^{N}\int d\boldsymbol{z}\,R^{\boldsymbol{\theta}}_{\phi_k(\boldsymbol{z})}(\omega)\,\left[A^{\phi}(\boldsymbol{z})^{-1}\right]_{kl}\,\left[R^{\boldsymbol{\theta}}_{\phi_l(\boldsymbol{z})}(\omega)\right]^{\dagger}. \tag{42}$$

Equation (42) is the frequency-domain FRR for general observables in overdamped Langevin systems. It is the Langevin realization of the relation stated in Sec. II; cf. (4). Its meaning is transparent: the power spectrum is reconstructed from local responses to perturbations applied at each point in configuration space.

Equation (42) applies to purely state-dependent observables, purely current-like observables, and their mixtures. Moreover, the structure is independent of whether the perturbation acts on the force, the mobility, or the temperature; only the perturbation matrix $A^{\phi}(\boldsymbol{z})$ differs. This completes the construction of the frequency-domain FRR for overdamped Langevin systems. The corresponding derivation for Markov jump systems follows the same logic, but the local structure is organized over discrete edges rather than continuous configuration space.

IV. FLUCTUATION–RESPONSE THEORY IN MARKOV JUMP SYSTEMS

In this section, we construct the frequency-domain FRR for Markov jump systems. The logic parallels that of Sec. III, but the local structure is now organized over the edges of a transition network rather than over points in configuration space. We first specify the jump dynamics and the perturbations of interest. We then introduce the relevant observables, expressed in terms of empirical state indicators and empirical currents. The central object is a discrete excess propagator, which determines both local responses and two-point covariances. This structure leads first to a local FRR for empirical state indicators and empirical currents, and then, by linearity, to the FRR for general observables. Technical derivations are deferred to Appendix B.

A. Setup and notation

We consider a continuous-time Markov jump process on a finite set of states $n \in \{1, 2, \ldots, S\}$. Let $p_n(t)$ denote the probability of occupying state n at time t. The dynamics is governed by the master equation

$$\partial_t p_n(t) = \sum_{m(\neq n)} \big[W_{nm} p_m(t) - W_{mn} p_n(t)\big], \tag{43}$$

where W_{nm} is the transition rate from state m to state n. Introducing the rate matrix $\mathcal{W}$ with off-diagonal elements $[\mathcal{W}]_{nm} = W_{nm}$ $(n \neq m)$ and diagonal elements

$$[\mathcal{W}]_{nn} = -\sum_{m(\neq n)} W_{mn}, \tag{44}$$

Eq. (43) can be written compactly as

$$\partial_t \boldsymbol{p}(t) = \mathcal{W} \boldsymbol{p}(t), \tag{45}$$

where

$$\boldsymbol{p}(t) = \big(p_1(t), \ldots, p_S(t)\big)^{\mathsf{T}}. \tag{46}$$

To separate the kinetic and entropic aspects of the dynamics, we parametrize the transition rates as

$$W_{nm} = \exp\left(B_{nm} + \frac{F_{nm}}{2}\right), \tag{47}$$

where $B_{nm} = B_{mn}$ and $F_{nm} = -F_{mn}$. Here, B_{nm} is the symmetric part of the rate and controls the kinetic timescale of the transition, while F_{nm} is the antisymmetric part and encodes the thermodynamic bias associated with the transition. This decomposition is commonly used in recent nonequilibrium fluctuation–response theory for jump processes [30–33].

We assume that the process is irreducible and admits a unique stationary distribution π_n, satisfying

$$\sum_m [\mathcal{W}]_{nm} \pi_m = 0. \tag{48}$$

The stationary distribution is the discrete analog of the steady-state density in the Langevin setting. The nonequilibrium character of the stationary state is reflected in the steady-state current along the edge $m \leftrightarrow n$,

$$j_{nm} = W_{nm}\pi_m - W_{mn}\pi_n, \tag{49}$$

which characterizes the net probability flow. By constrast, the corresponding traffic [39],

$$a_{nm} = W_{nm}\pi_m + W_{mn}\pi_n, \tag{50}$$

quantifies the total transition rate along that edge, irrespective of direction.

We consider local perturbations of the edge parameters B_{nm} and F_{nm}. For a perturbation on a specific edge $k \leftrightarrow l$, we take

$$B_{kl} \mapsto B_{kl} + \epsilon\, \delta(t - s), \tag{51}$$

or

$$F_{kl} \mapsto F_{kl} + \epsilon\, \delta(t - s), \tag{52}$$

for kinetic or entropic perturbations, respectively. These local impulsive perturbations are the discrete counterparts of the spatially localized perturbations introduced in Sec. III. Global perturbations can also be considered, for example $\boldsymbol{F} \mapsto \boldsymbol{F} + \epsilon\boldsymbol{\psi}$, for which the response is obtained as a linear combination of the corresponding local edge responses, as discussed below.

B. Observables, empirical fields, and response functions

We introduce empirical state indicators and currents as the discrete counterparts of the empirical stochastic fields in the Langevin setting. As in Sec. III, the goal is to treat state-dependent and current-like observables within a common framework.

For each state n, we define the state indicator

$$\eta_n(t) \equiv \delta_{X(t),n}, \tag{53}$$

where $X(t)$ denotes the state occupied by the system at time t. The variable $\eta_n(t)$ takes the value 1 when the system is in state n and 0 otherwise. These indicators are the discrete analog of the empirical density field (16).

To describe transitions, let $N_{nm}(t)$ denote the accumulated number of jumps from state m to state n up to time t. The corresponding empirical current on the edge $m \leftrightarrow n$ is defined by

$$\jmath_{nm}(t) \equiv \dot{N}_{nm}(t) - \dot{N}_{mn}(t), \tag{54}$$

where the overdot denotes the time derivative. This quantity is antisymmetric in n and m, and measures the instantaneous net jump current along the edge.

We consider a broad class of observables that are linear combinations of state indicators and empirical currents. For a single observable,

$$\theta(t) = \sum_{n=1}^{S} g_n\, \eta_n(t) + \sum_{n>m} \Lambda_{nm}\, \jmath_{nm}(t). \tag{55}$$

More generally, for a collection of N_O observables we write

$$\boldsymbol{\theta}(t) = G\,\boldsymbol{\eta}(t) + L\,\boldsymbol{\jmath}(t), \tag{56}$$

where

$$\boldsymbol{\eta}(t) = \big(\eta_1(t), \ldots, \eta_S(t)\big)^{\mathsf{T}} \tag{57}$$

is the state-indicator vector, and $\boldsymbol{\jmath}(t)$ is the vector of empirical edge currents, whose components are indexed by unoriented edges with a fixed convention, such as $n > m$. The matrix G contains the coefficients of the state-dependent part, while L contains the coefficients of the current-like part.

The covariance notation introduced in Eq. (1) applies directly to the discrete empirical fields. In particular, the two-point covariance functions are $C_{\eta_n,\eta_m}(\omega)$, $C_{\eta_n,\jmath_{kl}}(\omega)$, and $C_{\jmath_{nm},\jmath_{kl}}(\omega)$. The power spectrum matrix of the observable vector is $C_{\boldsymbol{\theta},\boldsymbol{\theta}^\mathsf{T}}(\omega)$. Thus, as in the continuous case, the fluctuation-response theory of general observables reduces to that of the elementary empirical observables $\eta_n(t)$ and $\jmath_{nm}(t)$.

We next define the corresponding local responses. Since the local perturbations act on edges, the relevant responses are those to perturbations of the symmetric and antisymmetric edge parameters B_{kl} and F_{kl}. For a local perturbation of the edge $k \leftrightarrow l$, the frequency-domain response of an observable A is

$$R^A_{B_{kl}}(\omega) = \int_0^\infty \frac{\delta\langle A(t)\rangle}{\delta B_{kl}(0)} e^{i\omega t}\, dt, \tag{58}$$

and

$$R^A_{F_{kl}}(\omega) = \int_0^\infty \frac{\delta\langle A(t)\rangle}{\delta F_{kl}(0)} e^{i\omega t}\, dt. \tag{59}$$

The response of a general observable follows from linearity. In particular,

$$R^{\boldsymbol{\theta}}_{F_{kl}}(\omega) = G\, R^{\boldsymbol{\eta}}_{F_{kl}}(\omega) + L\, R^{\boldsymbol{\jmath}}_{F_{kl}}(\omega), \tag{60}$$

and similarly for perturbations of B_{kl}. For a global perturbation of the antisymmetric part of the rates,

$$\boldsymbol{F} \mapsto \boldsymbol{F} + \epsilon \boldsymbol{\psi}, \tag{61}$$

the corresponding response is given by the linear combination of the local edge responses:

$$R^A_{\boldsymbol{F}\mapsto\boldsymbol{F}+\epsilon\boldsymbol{\psi}}(\omega) = \sum_{n>m} \psi_{nm}\, R^A_{F_{nm}}(\omega), \tag{62}$$

and analogously for perturbations of $\boldsymbol{B}$.

C. Excess propagator and local responses

We introduce the discrete counterpart of the excess propagator used in Sec. III C. As before, this object determines both the relaxation of the unperturbed dynamics and the local linear responses to impulsive perturbations.

The conditional probability of being in state n at time t, given that the system was in state k at time 0, is

$$P(n,t|k,0) = \left[e^{\mathcal{W}t}\right]_{nk}. \tag{63}$$

We define the excess propagator by [38]

$$H_{nk}(\omega) = \int_0^\infty \Big([e^{\mathcal{W}t}]_{nk} - \pi_n\Big) e^{i\omega t}\, dt. \tag{64}$$

This quantity is the discrete analog of the excess propagator (22): it measures the excess occupation of state n relative to the stationary state, induced by a localized initial condition at state k, at frequency ω.

The excess propagator satisfies the identities

$$\sum_m H_{nm}(\omega)\pi_m = 0, \tag{65}$$

$$\sum_m \big(i\omega\delta_{nm} + \mathcal{W}_{nm}\big) H_{mk}(\omega) = -\delta_{nk} + \pi_n, \tag{66}$$

and

$$\sum_m H_{nm}(\omega)\big(i\omega\delta_{mk} + \mathcal{W}_{mk}\big) = -\delta_{nk} + \pi_n. \tag{67}$$

These relations are the discrete counterparts of Eqs. (23)–(25). They show that $H_{nk}(\omega)$ is the projected resolvent of the Markov generator. Derivations are given in Appendix B 2.

We first consider an entropic perturbation of the edge $k \leftrightarrow l$, given by $F_{kl} \mapsto F_{kl} + \epsilon\,\delta(t)$. The corresponding response of the state indicator is

$$R^{\eta_n}_{F_{kl}}(\omega) = \int_0^\infty \frac{\delta\langle \eta_n(t)\rangle}{\delta F_{kl}(0)} e^{i\omega t}\, dt. \tag{68}$$

A direct calculation gives

$$R^{\eta_n}_{F_{kl}}(\omega) = \frac{a_{kl}}{2}\Big[H_{nk}(\omega) - H_{nl}(\omega)\Big]. \tag{69}$$

For a kinetic perturbation, $B_{kl} \mapsto B_{kl} + \epsilon\,\delta(t)$, we finds analogously

$$R^{\eta_n}_{B_{kl}}(\omega) = j_{kl}\Big[H_{nk}(\omega) - H_{nl}(\omega)\Big]. \tag{70}$$

Thus the two responses are proportional [30, 34, 37],

$$\frac{1}{j_{kl}} R^{\eta_n}_{B_{kl}}(\omega) = \frac{2}{a_{kl}} R^{\eta_n}_{F_{kl}}(\omega). \tag{71}$$

We next turn to the response of the empirical current. For a fixed edge $m \leftrightarrow n$, define

$$R^{\jmath_{nm}}_{F_{kl}}(\omega) = \int_0^\infty \frac{\delta\langle \jmath_{nm}(t)\rangle}{\delta F_{kl}(0)} e^{i\omega t}\, dt, \tag{72}$$

and similarly for $R^{\jmath_{nm}}_{B_{kl}}(\omega)$. These responses are expressed through the same excess propagator:

$$\frac{2}{a_{kl}} R^{\jmath_{nm}}_{F_{kl}}(\omega) = \frac{1}{j_{kl}} R^{\jmath_{nm}}_{B_{kl}}(\omega) \tag{73}$$

with

$$\frac{2}{a_{kl}} R^{\jmath_{nm}}_{F_{kl}}(\omega) = \delta_{nk}\delta_{ml} - \delta_{nl}\delta_{mk} \tag{74}$$
$$+ W_{nm}\Big[H_{mk}(\omega) - H_{ml}(\omega)\Big] - W_{mn}\Big[H_{nk}(\omega) - H_{nl}(\omega)\Big].$$

The first term in (74) is the direct local contribution from the impulsive perturbation acting on the perturbed edge, while the remaining terms describe how the perturbation propagates through the network and contributes to the current on the observed edge. The derivations of (69), (70), and (74) are given in Appendix B 1.

Equations (69)–(74) show that both the state and current response are determined by the same excess propagator $H_{nk}(\omega)$. In the state response, the relevant object is the difference $H_{nk}(\omega) - H_{nl}(\omega)$. In the current response, the same difference appears, but combined with transition rates in a way that reflects how excess occupation is converted into current along an edge.

D. Local fluctuation–response relation for empirical state and current

We turn from local responses to fluctuations. As in Sec. III D, the aim is to express the covariance functions of the elementary empirical observables in terms of the same local responses derived above. This yields the local form of the frequency-domain FRR for Markov jump systems.

A direct calculation yields the state–state covariance

$$C_{\eta_n,\eta_m}(\omega) = H_{nm}(\omega)\pi_m + H_{mn}(-\omega)\pi_n. \tag{75}$$

The crucial step is a discrete identity that rewrites (75) as a quadratic form

$$C_{\eta_n,\eta_m}(\omega) \tag{76}$$
$$= \sum_{k>l} a_{kl}\Big[H_{nk}(\omega) - H_{nl}(\omega)\Big]\Big[H_{mk}(-\omega) - H_{ml}(-\omega)\Big].$$

This identity is the discrete counterpart of Eq. (32). Its proof is deferred to Appendix B 4.

To express (76) in terms of response functions, we define the edge weights

$$A^F_{kl} = \frac{a_{kl}}{4}, \qquad A^B_{kl} = \frac{j^2_{kl}}{a_{kl}}. \tag{77}$$

Using Eqs. (69) and (70), the state–state covariance can then be written as

$$C_{\eta_n,\eta_m}(\omega) = \sum_{k>l} \frac{1}{A^\phi_{kl}} R^{\eta_n}_{\phi_{kl}}(\omega)\, R^{\eta_m}_{\phi_{kl}}(-\omega), \tag{78}$$

where $\phi \in \{F, B\}$ and A^ϕ_{kl} is defined accordingly.

The same logic applies to the mixed state–current covariance. We obtain

$$C_{\eta_n,\jmath_{n'm'}}(\omega) = \sum_{k>l} \frac{1}{A^\phi_{kl}} R^{\eta_n}_{\phi_{kl}}(\omega)\, R^{\jmath_{n'm'}}_{\phi_{kl}}(-\omega), \tag{79}$$

and an analogous expression holds for the current–current covariance:

$$C_{\jmath_{nm},\jmath_{n'm'}}(\omega) = \sum_{k>l} \frac{1}{A^\phi_{kl}} R^{\jmath_{nm}}_{\phi_{kl}}(\omega)\, R^{\jmath_{n'm'}}_{\phi_{kl}}(-\omega). \tag{80}$$

Equations (78)–(80) constitute the local frequency-domain FRR for Markov jump systems. The proofs of (79) and (80) are deferred to Appendix B 3.

Three features are worth emphasizing. First, the local FRR shows that fluctuations at frequency ω are controlled by the system's response at the same frequency to perturbations of individual edges. The spectrum thus acquires a direct edgewise interpretation. Second, the perturbation type enters only through the scalar weight A^ϕ_{kl}, while the dynamical information is contained in the local responses themselves. Third, because the decomposition is organized over edges, the jump-process formulation naturally identifies which transition channels dominate a given spectral feature.

E. Frequency-domain fluctuation–response relation for general observables

With the local FRRs established, the extension to general observables is immediate. As in Sec. III E, both the response and the covariance of a general observable follow from combining the corresponding local quantities of the elementary empirical variables. The combination is determined by the coefficients defining the observable.

Given the form (56) of the observable vector, its local response to a perturbation of the edge parameter ϕ_{kl} is given by

$$R^{\boldsymbol{\theta}}_{\phi_{kl}}(\omega) = G\, R^{\boldsymbol{\eta}}_{\phi_{kl}}(\omega) + L\, R^{\boldsymbol{\jmath}}_{\phi_{kl}}(\omega), \tag{81}$$

where

$$R^{\boldsymbol{\eta}}_{\phi_{kl}}(\omega) = \big(R^{\eta_1}_{\phi_{kl}}(\omega), \ldots, R^{\eta_S}_{\phi_{kl}}(\omega)\big)^\mathsf{T}, \tag{82}$$

and similarly for $R^{\boldsymbol{\jmath}}_{\phi_{kl}}(\omega)$.

The covariance of $\boldsymbol{\theta}(t)$ follows from (56):

$$\begin{aligned} C_{\boldsymbol{\theta},\boldsymbol{\theta}^\mathsf{T}}(\omega) &= G\, C_{\boldsymbol{\eta},\boldsymbol{\eta}^\mathsf{T}}(\omega)\, G^\mathsf{T} + G\, C_{\boldsymbol{\eta},\boldsymbol{\jmath}^\mathsf{T}}(\omega)\, L^\mathsf{T} \\ &\quad + L\, C_{\boldsymbol{\jmath},\boldsymbol{\eta}^\mathsf{T}}(\omega)\, G^\mathsf{T} + L\, C_{\boldsymbol{\jmath},\boldsymbol{\jmath}^\mathsf{T}}(\omega)\, L^\mathsf{T}. \end{aligned} \tag{83}$$

Substituting (78)–(80) into (83) and using (81), we obtain

$$C_{\boldsymbol{\theta},\boldsymbol{\theta}^\mathsf{T}}(\omega) = \sum_{k>l} \frac{1}{A^\phi_{kl}} R^{\boldsymbol{\theta}}_{\phi_{kl}}(\omega)\, \big[R^{\boldsymbol{\theta}}_{\phi_{kl}}(\omega)\big]^\dagger. \tag{84}$$

Equation (84) is the frequency-domain FRR for general observables in Markov jump systems. It is the jump-process realization of the unified relation stated in Sec. II; cf. (5).

The interpretation of (84) is transparent in the network setting. The fluctuation spectrum is decomposed into contributions from the responses to perturbations of individual edges. The FRR provides an explicit edge-wise interpretation of how the network dynamics shapes the fluctuation spectrum. As in the Langevin case, the relation applies uniformly to purely state-dependent observables, purely current-like observables, and their combinations. The distinction between kinetic and entropic perturbations enters only through the edge weight A^{ϕ}_{kl}, while the dynamical information is carried by the local responses themselves.

This completes the frequency-domain FRR for Markov jump systems. Taken together, Secs. III and IV show that a common underlying structure governs both continuous and discrete nonequilibrium dynamics.

V. CONSEQUENCES OF THE FREQUENCY-DOMAIN FLUCTUATION–RESPONSE RELATION

In this section, we derive the main consequences of the frequency-domain FRR. Rather than treating these results as separate statements, we show that they arise from a common structure. The RUR follows directly from the quadratic form of the frequency-domain FRR; the response KUR and TUR follow from specific perturbation choices; the FDT together with Harada–Sasa-type relations arise as two reductions of the same identity, corresponding to equilibrium and nonequilibrium conditions, respectively. To keep the section focused on the physical content, detailed algebraic manipulations are deferred to Appendix C.

A. Frequency-domain response uncertainty relation

A direct consequence of the frequency-domain FRR is a bound on the response to an arbitrary global perturbation. This bound follows from the Cauchy–Schwarz inequality applied to the quadratic response representation of the power spectrum. It provides a frequency-resolved trade-off between the magnitude of the response and the spontaneous fluctuations of the corresponding observable.

We first consider the overdamped Langevin case. For a global perturbation of $\phi \in \{\boldsymbol{F}, \ln M, T\}$ of the form $\phi_k(\boldsymbol{x}) \mapsto \phi_k(\boldsymbol{x}) + \epsilon\, \psi_k(\boldsymbol{x}, t)$, the corresponding response of the observable vector $\boldsymbol{\theta}(t)$ is given by

$$R^{\boldsymbol{\theta}}_{\phi\mapsto\phi+\epsilon\boldsymbol{\psi}}(\omega) = \sum_{k=1}^{N} \int d\boldsymbol{x}\, \psi_k(\boldsymbol{x}, \omega)\, R^{\boldsymbol{\theta}}_{\phi_k(\boldsymbol{x})}(\omega). \tag{85}$$

Applying the Cauchy–Schwarz inequality to the FRR (42) yields (see Appendix C 1 for details)

$$\begin{aligned}&\left[R^{\boldsymbol{\theta}}_{\phi\mapsto\phi+\epsilon\boldsymbol{\psi}}(\omega)\right]^{\dagger} C_{\boldsymbol{\theta},\boldsymbol{\theta}^{\mathsf{T}}}(\omega)^{-1} R^{\boldsymbol{\theta}}_{\phi\mapsto\phi+\epsilon\boldsymbol{\psi}}(\omega)\\ &\leq \sum_{k,l=1}^{N} \int d\boldsymbol{x}\, \psi_k(\boldsymbol{x}, -\omega) A^{\phi}_{kl}(\boldsymbol{x}) \psi_l(\boldsymbol{x}, \omega),\end{aligned} \tag{86}$$

For a single observable $\theta(t)$, this inequality reduces to

$$\begin{aligned}&\left|R^{\theta}_{\phi\mapsto\phi+\epsilon\boldsymbol{\psi}}(\omega)\right|^2\\ &\leq C_{\theta,\theta}(\omega) \sum_{k,l=1}^{N} \int d\boldsymbol{x}\, \psi_k(\boldsymbol{x}, -\omega) A^{\phi}_{kl}(\boldsymbol{x}) \psi_l(\boldsymbol{x}, \omega).\end{aligned} \tag{87}$$

The same logic applies to Markov jump systems. For a global perturbation of either the symmetric or antisymmetric edge parameter, $\phi_{nm} \mapsto \phi_{nm} + \epsilon\, \psi_{nm}(t)$ ($\phi \in \{B, F\}$), the corresponding response of the observable vector $\boldsymbol{\theta}(t)$ is given by

$$R^{\boldsymbol{\theta}}_{\phi\mapsto\phi+\epsilon\boldsymbol{\psi}}(\omega) = \sum_{n>m} \psi_{nm}(\omega) R^{\boldsymbol{\theta}}_{\phi_{nm}}(\omega). \tag{88}$$

Applying the Cauchy–Schwarz inequality to (84) yields (see Appendix C 1 for details)

$$\begin{aligned}&\left[R^{\boldsymbol{\theta}}_{\phi\mapsto\phi+\epsilon\boldsymbol{\psi}}(\omega)\right]^{\dagger} C_{\boldsymbol{\theta},\boldsymbol{\theta}^{\mathsf{T}}}(\omega)^{-1} R^{\boldsymbol{\theta}}_{\phi\mapsto\phi+\epsilon\boldsymbol{\psi}}(\omega)\\ &\leq \sum_{n>m} A^{\phi}_{nm} \left|\psi_{nm}(\omega)\right|^2 .\end{aligned} \tag{89}$$

For a single observable $\theta(t)$, this reduces to

$$\left|R^{\theta}_{\phi\mapsto\phi+\epsilon\boldsymbol{\psi}}(\omega)\right|^2 \leq C_{\theta,\theta}(\omega) \sum_{n>m} A^{\phi}_{nm} \left|\psi_{nm}(\omega)\right|^2. \tag{90}$$

Equations (86) and (89) are the frequency-domain RURs. In both continuous and discrete dynamics, the response at frequency ω is determined by two ingredients: the power spectrum of the observable at that frequency, and a quadratic cost associated with the perturbation. The only difference lies in how locality is organized: over configuration space in the Langevin case, and over edges in the jump-process case.

B. Frequency-domain response kinetic and thermodynamic uncertainty relations

The bounds derived in Sec. V A become more informative once the perturbation class is fixed. In that case, the perturbation weight matrix A^{ϕ} admits a clear physical meaning, leading to uncertainty relations governed by kinetic or thermodynamic quantities.

We begin with overdamped Langevin systems. For a force perturbation, $\boldsymbol{F}(\boldsymbol{x}) \mapsto \boldsymbol{F}(\boldsymbol{x}) + \epsilon\, \boldsymbol{\psi}(\boldsymbol{x}, t)$, the weight matrix follows from (36) using (A20):

$$[A^{\boldsymbol{F}}(\boldsymbol{x})]_{kl} = \delta_{kl}\, \frac{\pi(\boldsymbol{x})\mu_k(\boldsymbol{x})}{2T_k(\boldsymbol{x})}. \tag{91}$$

Substituting (91) into (86) gives

$$\begin{aligned} &\left[R^{\boldsymbol{\theta}}_{\boldsymbol{F}\mapsto\boldsymbol{F}+\epsilon\boldsymbol{\psi}}(\omega)\right]^{\dagger} C_{\boldsymbol{\theta},\boldsymbol{\theta}^{\mathsf{T}}}(\omega)^{-1} R^{\boldsymbol{\theta}}_{\boldsymbol{F}\mapsto\boldsymbol{F}+\epsilon\boldsymbol{\psi}}(\omega) \qquad (92)\\ &\le \sum_{k=1}^{N} \int d\boldsymbol{x}\, \frac{\pi(\boldsymbol{x})\mu_k(\boldsymbol{x})}{2T_k(\boldsymbol{x})} |\psi_k(\boldsymbol{x},\omega)|^2. \end{aligned}$$

Bounding the perturbation amplitude by $|\psi_k(\boldsymbol{x},\omega)| \le \psi_{\max}$, the inequality (92) further reduces to the compact, albeit looser, bound:

$$\begin{aligned} &\left[R^{\boldsymbol{\theta}}_{\boldsymbol{F}\mapsto\boldsymbol{F}+\epsilon\boldsymbol{\psi}}(\omega)\right]^{\dagger} C_{\boldsymbol{\theta},\boldsymbol{\theta}^{\mathsf{T}}}(\omega)^{-1} R^{\boldsymbol{\theta}}_{\boldsymbol{F}\mapsto\boldsymbol{F}+\epsilon\boldsymbol{\psi}}(\omega) \qquad (93)\\ &\le \psi_{\max}^2 \sum_{k=1}^{N} \left\langle \frac{\mu_k(\boldsymbol{x})}{2T_k(\boldsymbol{x})} \right\rangle_{\rm ss}. \end{aligned}$$

This bound constitutes the frequency-domain extension of the response KUR for overdamped Langevin dynamics [34], which was originally derived for Markov jump processes in the time domain [29, 33]. The finite-frequency fluctuation–response inequality found in [35] is recovered as a special case under separable perturbations, i.e., $\boldsymbol{\psi}(\boldsymbol{x},t) = \sum_q \boldsymbol{g}_q(\boldsymbol{x})\phi_q(t)$, with spatial modes $\boldsymbol{g}_q(\boldsymbol{x})$ and temporal amplitudes $\phi_q(t)$.

For linear Langevin systems with spatially uniform M and T, and a force $\boldsymbol{F}(\boldsymbol{x}) = -A\boldsymbol{x}$, the power spectrum is known to be $C_{\boldsymbol{x},\boldsymbol{x}^{\mathsf{T}}}(\omega) = 2(MA - i\omega I)^{-1} D[(MA + i\omega I)^{\mathsf{T}}]^{-1}$ [36, 40]. The response function to a homogeneous force perturbation $\boldsymbol{F}(\boldsymbol{x}) \mapsto \boldsymbol{F}(\boldsymbol{x}) + \epsilon\boldsymbol{\psi}$ is readily obtained as $R^{\boldsymbol{x}}_{\boldsymbol{F}\mapsto\boldsymbol{F}+\epsilon\boldsymbol{\psi}}(\omega) = (MA - i\omega I)^{-1} M\boldsymbol{\psi}$. Thus, the response KUR is saturated in this case: $[R^{\boldsymbol{x}}_{\boldsymbol{F}\mapsto\boldsymbol{F}+\epsilon\boldsymbol{\psi}}(\omega)]^{\dagger} C_{\boldsymbol{x},\boldsymbol{x}^{\mathsf{T}}}(\omega)^{-1} R^{\boldsymbol{x}}_{\boldsymbol{F}\mapsto\boldsymbol{F}+\epsilon\boldsymbol{\psi}}(\omega) = \boldsymbol{\psi}^{\mathsf{T}} M (2T)^{-1}\boldsymbol{\psi}$. This saturation has been recently verified algebraically in [35, 36]. In contrast, the equality condition of the Cauchy–Schwarz inequality [Eqs. (C6) and (C14)] shows that the saturation arises as a structural consequence of the frequency-domain FRR. This perspective not only explains the saturation of the response KUR in linear Langevin systems, but also provides a potential route to identifying saturation conditions for other response uncertainty relations and more general settings.

A second important choice is the mobility perturbation, $\ln M(\boldsymbol{x}) \mapsto \ln M(\boldsymbol{x}) + \epsilon\, \boldsymbol{\psi}(\boldsymbol{x},t)$. In this case, the weight matrix is determined by the steady-state current, and (86) becomes

$$\begin{aligned} &\left[R^{\boldsymbol{\theta}}_{\ln M\mapsto\ln M+\epsilon\boldsymbol{\psi}}(\omega)\right]^{\dagger} C_{\boldsymbol{\theta},\boldsymbol{\theta}^{\mathsf{T}}}(\omega)^{-1} R^{\boldsymbol{\theta}}_{\ln M\mapsto\ln M+\epsilon\boldsymbol{\psi}}(\omega) \qquad (94)\\ &\le \sum_{k=1}^{N} \int d\boldsymbol{x}\, \frac{[j_k^{\rm ss}(\boldsymbol{x})]^2}{2\pi(\boldsymbol{x})D_k(\boldsymbol{x})} |\psi_k(\boldsymbol{x},\omega)|^2. \end{aligned}$$

Bounding the perturbation amplitude by $|\psi_k(\boldsymbol{x},\omega)| \le \psi_{\max}$, this implies

$$\begin{aligned} &\left[R^{\boldsymbol{\theta}}_{\ln M\mapsto\ln M+\epsilon\boldsymbol{\psi}}(\omega)\right]^{\dagger} C_{\boldsymbol{\theta},\boldsymbol{\theta}^{\mathsf{T}}}(\omega)^{-1} R^{\boldsymbol{\theta}}_{\ln M\mapsto\ln M+\epsilon\boldsymbol{\psi}}(\omega) \qquad (95)\\ &\le \psi_{\max}^2\, \frac{\sigma}{2}, \end{aligned}$$

where

$$\sigma = \sum_{k=1}^{N} \int d\boldsymbol{x}\, \frac{[j_k^{\rm ss}(\boldsymbol{x})]^2}{\pi(\boldsymbol{x})D_k(\boldsymbol{x})} \tag{96}$$

is the entropy production rate. This bound constitutes the frequency-domain extension of the response TUR for overdamped Langevin dynamics [33, 34]. The response KUR and TUR complement each other by bounding the response–fluctuation ratio in terms of quantities characterizing kinetic and thermodynamic aspects of nonequilibrium systems.

A particularly important specialization of (95) is obtained for current-like observables under a homogeneous mobility perturbation, $\psi_k(\boldsymbol{x},\omega) = 1$ (for all k, $\boldsymbol{x}$, and ω). In that case, the global response reduces to the steady-state mean of the observable. This follows because the homogeneous perturbation rescales the steady-state current uniformly, as can be seen from (17), (19), and (21) with $G(\boldsymbol{x}) = 0$:

$$R^{\boldsymbol{\theta}}_{\ln M\mapsto\ln M+\epsilon}(\omega) = \langle\boldsymbol{\theta}\rangle_{\rm ss}, \tag{97}$$

and (95) becomes

$$\langle\boldsymbol{\theta}\rangle_{\rm ss}^{\mathsf{T}} C_{\boldsymbol{\theta},\boldsymbol{\theta}^{\mathsf{T}}}(\omega)^{-1} \langle\boldsymbol{\theta}\rangle_{\rm ss} \le \frac{\sigma}{2}. \tag{98}$$

(See Appendix C 2 for more details.) Equation (98) is the frequency-domain TUR for overdamped Langevin systems. It extends the multidimensional TUR of [41] to finite frequencies by replacing the covariance with the power spectrum. In contrast to the conventional TUR, which involves the frequency-integrated covariance, this bound holds at each frequency, providing a frequency-resolved constraint while the entropy production remains frequency-independent.

We now turn to Markov jump systems. For an entropic perturbation, $F_{nm} \mapsto F_{nm} + \epsilon\, \psi_{nm}(t)$, substituting (77) into (89) yields

$$\left[R^{\boldsymbol{\theta}}_{\boldsymbol{F}\mapsto\boldsymbol{F}+\epsilon\boldsymbol{\psi}}(\omega)\right]^{\dagger} C_{\boldsymbol{\theta},\boldsymbol{\theta}^{\mathsf{T}}}(\omega)^{-1} R^{\boldsymbol{\theta}}_{\boldsymbol{F}\mapsto\boldsymbol{F}+\epsilon\boldsymbol{\psi}}(\omega) \le \sum_{n>m} \frac{a_{nm}}{4}\,|\psi_{nm}(\omega)|^2. \tag{99}$$

Bounding the perturbation amplitude by $|\psi_{nm}(\omega)| \le \psi_{\max}$, (99) reduces to

$$\left[R^{\boldsymbol{\theta}}_{\boldsymbol{F}\mapsto\boldsymbol{F}+\epsilon\boldsymbol{\psi}}(\omega)\right]^{\dagger} C_{\boldsymbol{\theta},\boldsymbol{\theta}^{\mathsf{T}}}(\omega)^{-1} R^{\boldsymbol{\theta}}_{\boldsymbol{F}\mapsto\boldsymbol{F}+\epsilon\boldsymbol{\psi}}(\omega) \le \psi_{\max}^2\,\frac{\mathcal{A}}{4}, \tag{100}$$

where

$$\mathcal{A} = \sum_{n>m} a_{nm} \tag{101}$$

is the dynamical activity, characterizing the time-symmetric aspect of the dynamics [42]. This bound extends the response KUR for Markov jump systems to the frequency domain [29, 33].

For a kinetic perturbation, $B_{nm} \mapsto B_{nm} + \epsilon\,\psi_{nm}(t)$, substituting (77) into (89) yields

$$\left[R^{\boldsymbol{\theta}}_{\boldsymbol{B}\mapsto\boldsymbol{B}+\epsilon\boldsymbol{\psi}}(\omega)\right]^{\dagger} C_{\boldsymbol{\theta},\boldsymbol{\theta}^{\mathsf{T}}}(\omega)^{-1} R^{\boldsymbol{\theta}}_{\boldsymbol{B}\mapsto\boldsymbol{B}+\epsilon\boldsymbol{\psi}}(\omega) \le \sum_{n>m} \frac{j_{nm}^2}{a_{nm}}\,|\psi_{nm}(\omega)|^2. \tag{102}$$

Introducing the pseudo-entropy production rate

$$\sigma^{\mathrm{ps}} = 2\sum_{n>m}\frac{j_{nm}^2}{a_{nm}}, \tag{103}$$

Bounding the perturbation amplitude by $|\psi_{nm}(\omega)| \le \psi_{\max}$, this yields

$$\left[R^{\boldsymbol{\theta}}_{\boldsymbol{B}\mapsto\boldsymbol{B}+\epsilon\boldsymbol{\psi}}(\omega)\right]^{\dagger} C_{\boldsymbol{\theta},\boldsymbol{\theta}^{\mathsf{T}}}(\omega)^{-1} R^{\boldsymbol{\theta}}_{\boldsymbol{B}\mapsto\boldsymbol{B}+\epsilon\boldsymbol{\psi}}(\omega) \le \psi_{\max}^2\,\frac{\sigma^{\mathrm{ps}}}{2}. \tag{104}$$

This bound extends the response TKUR for Markov jump systems to the frequency domain [33].

As in the Langevin case, a direct bound on the mean value of a current-like observable is obtained by a homogeneous kinetic perturbation, $\psi_{nm}(\omega) = 1$ (for all $n > m$ and ω). For current-like observables, the corresponding global response reduces to the stationary mean,

$$R^{\boldsymbol{\theta}}_{\boldsymbol{B}\mapsto\boldsymbol{B}+\epsilon}(\omega) = \langle\boldsymbol{\theta}\rangle_{\mathrm{ss}}, \tag{105}$$

and (104) becomes

$$\langle\boldsymbol{\theta}\rangle_{\mathrm{ss}}^{\mathsf{T}} C_{\boldsymbol{\theta},\boldsymbol{\theta}^{\mathsf{T}}}(\omega)^{-1}\langle\boldsymbol{\theta}\rangle_{\mathrm{ss}} \le \frac{\sigma^{\mathrm{ps}}}{2}. \tag{106}$$

This bound extends the multidimensional TKUR for Markov jump systems to the frequency domain [20].

Equations (93)–(106) show that the response bound derived in Sec. V A gives rise to a family of concrete inequalities whose right-hand sides are determined by mobility, dynamical activity, entropy production, and pseudo-entropy production, depending on the perturbation class. These results demonstrate that familiar uncertainty relations of nonequilibrium thermodynamics can be viewed as arising from a common frequency-domain fluctuation–response structure under suitable physical choices of perturbation [28, 30, 33, 34].

C. Equilibrium limit: fluctuation–dissipation theorem

The frequency-domain FRR reduces to the equilibrium FDT when the steady irreversible currents vanish and the local response satisfies the reciprocity relation. In the present framework, this can be shown directly in the main text, while proofs of the reciprocity identities are deferred to Appendix C 3.

We begin with the overdamped Langevin case. For force perturbations, combining (29), (30), and (A20) yields

$$R^{\boldsymbol{\jmath}(\boldsymbol{x})}_{\boldsymbol{F}(\boldsymbol{z})}(\omega) = \mathcal{P}(\boldsymbol{x},\boldsymbol{z};\omega)\,M(\boldsymbol{z})\pi(\boldsymbol{z}). \tag{107}$$

Appendix C 4 shows that the current–current covariance can be rewritten as

$$C_{\boldsymbol{\jmath}(\boldsymbol{x}),\boldsymbol{\jmath}(\boldsymbol{z})^{\mathsf{T}}}(\omega) = R^{\boldsymbol{\jmath}(\boldsymbol{x})}_{\boldsymbol{F}(\boldsymbol{z})}(\omega)\,T(\boldsymbol{z}) + T(\boldsymbol{x})\left[R^{\boldsymbol{\jmath}(\boldsymbol{z})}_{\boldsymbol{F}(\boldsymbol{x})}(\omega)\right]^{\dagger} + \left[\hat{\mathcal{J}}_{\boldsymbol{x}}H(\boldsymbol{x},\boldsymbol{z};\omega)\right]\boldsymbol{j}_{\mathrm{ss}}(\boldsymbol{z})^{\mathsf{T}} + \boldsymbol{j}_{\mathrm{ss}}(\boldsymbol{x})\left[\hat{\mathcal{J}}_{\boldsymbol{z}}H(\boldsymbol{z},\boldsymbol{x};\omega)\right]^{\dagger}. \tag{108}$$

At equilibrium, the last two terms vanish since $\boldsymbol{j}_{\mathrm{ss}}(\boldsymbol{x}) = 0$, and time-reversal symmetry enforces the reciprocity relation

$$\left[R^{\boldsymbol{\jmath}(\boldsymbol{x})}_{\boldsymbol{F}(\boldsymbol{z})}(\omega)\right]_{\mathrm{eq}} = \left[R^{\boldsymbol{\jmath}(\boldsymbol{z})}_{\boldsymbol{F}(\boldsymbol{x})}(\omega)\right]^{\mathsf{T}}_{\mathrm{eq}}. \tag{109}$$

Therefore, for a spatially homogeneous temperature $T(\boldsymbol{x}) = T$, the expression (108) reduces in equilibrium to

$$\left[C_{\boldsymbol{\jmath}(\boldsymbol{x}),\boldsymbol{\jmath}(\boldsymbol{z})^{\mathsf{T}}}(\omega)\right]_{\mathrm{eq}} = 2T\,\mathrm{Re}\left[R^{\boldsymbol{\jmath}(\boldsymbol{x})}_{\boldsymbol{F}(\boldsymbol{z})}(\omega)\right]_{\mathrm{eq}}. \tag{110}$$

This is the local frequency-domain FDT for empirical currents. A current-like observable is a linear functional of the empirical current. Multiplying by the weight functions $L(\boldsymbol{x})$ and $L(\boldsymbol{z})$ and integrating over $\boldsymbol{x}$ and $\boldsymbol{z}$ yields the observable-level FDT for current-like observables. The proof of (109) is given in Appendix C 3.

The same logic applies to Markov jump systems. Appendix C 4 shows that the local current–current covariance can be rewritten as

$$C_{\jmath_{nm},\jmath_{n'm'}}(\omega) = R^{\jmath_{nm}}_{F_{n'm'}}(\omega) + R^{\jmath_{n'm'}}_{F_{nm}}(-\omega) + \Delta_{nm,n'm'}(\omega), \tag{111}$$

where $\Delta_{nm,n'm'}(\omega)$ is a term proportional to the steady currents and therefore vanishes at equilibrium. Its explicit definition is given in (C51) and (C53). At equilibrium,

$$j_{nm} = 0 \qquad \text{for all } n, m, \tag{112}$$

and time-reversal symmetry yields the reciprocity relation

$$\left[R^{\jmath_{nm}}_{F_{n'm'}}(\omega)\right]_{\rm eq} = \left[R^{\jmath_{n'm'}}_{F_{nm}}(\omega)\right]_{\rm eq}. \tag{113}$$

Substituting (113) into (111) gives

$$\left[C_{\jmath_{nm},\jmath_{n'm'}}(\omega)\right]_{\rm eq} = 2\mathrm{Re}\left[\mathrm{R}^{\jmath_{nm}}_{\mathrm{F}_{n'm'}}(\omega)\right]_{\rm eq}. \tag{114}$$

This is the equilibrium FDT for local edge currents in the Markov jump setting. A current-like observable is a linear combination of the edge currents. Multiplying (114) by the coefficients Λ_{nm} and $\Lambda_{n'm'}$ and summing over all edges yields the observable-level equilibrium FDT. The proof of (113) is given in Appendix C 3.

The equilibrium FDT is recovered when the current-dependent terms vanish. Away from equilibrium, these terms persist and encode the extent to which the equilibrium FDT is violated. We next show that this deviation can be expressed in a form related to dissipation.

D. FDT violation and Harada–Sasa relations

We isolate the current-dependent correction terms in the full nonequilibrium covariance–response identities (108) and (111). These terms quantify the violation of the FDT and are therefore responsible for the breakdown of the equilibrium reduction derived in Sec. V C. Integrating them over frequency yields Harada–Sasa-type relations [8, 9].

We first consider the overdamped Langevin case. Equation (108) shows that the deviation from the equilibrium FDT is carried by the two terms proportional to the steady-state current. Under spatially homogeneous mobility and temperature,

$$M(\boldsymbol{x}) = \mu I, \qquad T(\boldsymbol{x}) = T, \tag{115}$$

integrating (108) over $\boldsymbol{x}$ and $\boldsymbol{z}$ yields the covariance–response identity for the velocity observable $\dot{\boldsymbol{x}}(t)$:

$$\begin{aligned} &C_{\dot{\boldsymbol{x}},\dot{\boldsymbol{x}}^{\mathsf{T}}}(\omega) - T\,R^{\dot{\boldsymbol{x}}}_{\boldsymbol{F}\mapsto\boldsymbol{F}+\epsilon}(\omega) - T\left[R^{\dot{\boldsymbol{x}}}_{\boldsymbol{F}\mapsto\boldsymbol{F}+\epsilon}(\omega)\right]^{\dagger} \\ &= \mathcal{Z}(\omega) + \mathcal{Z}(\omega)^{\dagger}, \end{aligned} \tag{116}$$

where the current-dependent contribution $\mathcal{Z}(\omega)$ is given by

$$\mathcal{Z}(\omega) = \int d\boldsymbol{x} \int d\boldsymbol{z}\left[\hat{\mathcal{J}}_{\boldsymbol{x}} H(\boldsymbol{x},\boldsymbol{z};\omega)\right]\boldsymbol{j}_{\rm ss}(\boldsymbol{z})^{\mathsf{T}} \tag{117}$$

The left-hand side of (116) thus quantifies the frequency-resolved violation of the equilibrium FDT for the velocity observable.

Using the identity

$$\int_{-\infty}^{\infty} H(\boldsymbol{x},\boldsymbol{z};\omega)\,\frac{d\omega}{2\pi} = \frac{1}{2}\left[\delta(\boldsymbol{x}-\boldsymbol{z}) - \pi(\boldsymbol{x})\right], \tag{118}$$

the integrated correction term can be evaluated explicitly. Taking the trace of the resulting matrix identity gives

$$\begin{aligned} &\sum_{k=1}^{N}\int_{-\infty}^{\infty}\left[C_{\dot{x}_k,\dot{x}_k}(\omega) - 2T\,\mathrm{Re}\,R^{\dot{x}_k}_{F_k\mapsto F_k+\epsilon}(\omega)\right]\frac{d\omega}{2\pi} \\ &= \mu\,\langle\dot{Q}\rangle_{\rm ss} - \left|\langle\dot{\boldsymbol{x}}\rangle_{\rm ss}\right|^2, \end{aligned} \tag{119}$$

where

$$\langle\dot{Q}\rangle_{\rm ss} = \int d\boldsymbol{x}\,\boldsymbol{F}(\boldsymbol{x})^{\mathsf{T}}\boldsymbol{j}_{\rm ss}(\boldsymbol{x}) \tag{120}$$

is the steady-state heat dissipation rate [6]. Equation (119) is the Harada–Sasa relation, stating that the integrated violation of the FDT is determined by dissipation, up to the correction associated with the mean drift [8, 9]

A more general form can be obtained without assuming homogeneous mobility by introducing the current-like observable $\boldsymbol{w}(t) = M(\boldsymbol{x}(t))^{-1}\circ\dot{\boldsymbol{x}}(t)$. Applying the same procedure to the mixed covariance between $\boldsymbol{w}(t)$ and $\dot{\boldsymbol{x}}(t)$ yields

$$\begin{aligned} &\sum_{k=1}^{N}\int_{-\infty}^{\infty}\left[C_{\dot{x}_k,w_k}(\omega) - 2T\,\mathrm{Re}\,R^{w_k}_{F_k\mapsto F_k+\epsilon}(\omega)\right]\frac{d\omega}{2\pi} \\ &= \langle\dot{Q}\rangle_{\rm ss} - \langle\boldsymbol{w}\rangle_{\rm ss}^{\mathsf{T}}\langle\dot{\boldsymbol{x}}\rangle_{\rm ss}. \end{aligned} \tag{121}$$

This generalized Harada–Sasa relation was studied in [10], where the inhomogeneity of the mobility arises from hydrodynamic interactions.

A similar structure arises for Markov jump systems. Equation (111) shows that the deviation from the equilibrium FDT is encoded in the correction term $\Delta_{nm,n'm'}(\omega)$, which vanishes only when the steady currents vanish. To relate this edge-based microscopic identity to macroscopic physical observables, we reorganize the description in terms of cycle currents defined on a fundamental set of directed cycles [43, 44]. These cycle currents provide a minimal set of independent current-like observables, as symmetries and conservation laws render steady-state edge currents redundant [45, 46]. The corresponding thermodynamic forces defined on cycles, known as affinities, represent the physical driving forces that maintain the system out of equilibrium. Together, they form the appropriate current–force pairs at the macroscopic level. In particular, since edge currents are not independent, fluctuation–dissipation relations at equilibrium, as well as their violations away from equilibrium, are formulated in terms of these cycle-level observables [30, 47, 48]. Motivated by this structure, we consider a directed cycle $\mathcal{C}$

in the network, consisting of the edges

$$(\mathcal{C}_1,\mathcal{C}_2),\ (\mathcal{C}_2,\mathcal{C}_3),\ \ldots,\ (\mathcal{C}_{n_\mathcal{C}},\mathcal{C}_1). \tag{122}$$

The corresponding empirical cycle current is defined by

$$\jmath^{\mathcal{C}}(t)=\sum_{i=1}^{n_\mathcal{C}}\jmath_{\mathcal{C}_{i+1},\mathcal{C}_i}(t),\qquad \mathcal{C}_{n_\mathcal{C}+1}\equiv\mathcal{C}_1. \tag{123}$$

Summing (111) over all pairs of edges in the cycle yields the corresponding covariance–response identity for the cycle current,

$$C_{\jmath^\mathcal{C},\jmath^\mathcal{C}}(\omega)=R^{\jmath^\mathcal{C}}_{\boldsymbol{F}_\mathcal{C}\mapsto\boldsymbol{F}_\mathcal{C}+\epsilon}(\omega)+R^{\jmath^\mathcal{C}}_{\boldsymbol{F}_\mathcal{C}\mapsto\boldsymbol{F}_\mathcal{C}+\epsilon}(-\omega)+\Delta_\mathcal{C}(\omega), \tag{124}$$

where the perturbation acts homogeneously on all edges belonging to the cycle, and $\Delta_\mathcal{C}(\omega)$ is the corresponding cycle-summed correction term.

Using the identity

$$\int_{-\infty}^{\infty}H_{nm}(\omega)\,\frac{d\omega}{2\pi}=\frac{1}{2}(\delta_{nm}-\pi_n), \tag{125}$$

the frequency-integrated form of (124) yields

$$\begin{aligned}&\int_{-\infty}^{\infty}\Big[C_{\jmath^\mathcal{C},\jmath^\mathcal{C}}(\omega)-2\,\mathrm{Re}\,R^{\jmath^\mathcal{C}}_{\boldsymbol{F}_\mathcal{C}\mapsto\boldsymbol{F}_\mathcal{C}+\epsilon}(\omega)\Big]\frac{d\omega}{2\pi} \qquad (126)\\ &=\frac{1}{2}\sum_{i=1}^{n_\mathcal{C}}\Big[W_{\mathcal{C}_{i+1},\mathcal{C}_i}-W_{\mathcal{C}_{i-1},\mathcal{C}_i}\Big]\Big[j_{\mathcal{C}_{i+1},\mathcal{C}_i}+j_{\mathcal{C}_i,\mathcal{C}_{i-1}}\Big]-\big(J^\mathcal{C}\big)^2,\end{aligned}$$

where

$$J^\mathcal{C}=\sum_{i=1}^{n_\mathcal{C}}j_{\mathcal{C}_{i+1},\mathcal{C}_i} \tag{127}$$

is the stationary cycle current. Equation (126) can be viewed as a Harada–Sasa-type relation for Markov jump systems: the integrated violation of the equilibrium FDT is expressed in terms of steady-state currents and transition rates along the cycle, despite lacking a clear interpretation in terms of heat dissipation as in the Langevin case.

The physical content of (119)–(126) is closely analogous in both continuous and discrete dynamics. In equilibrium, the FDT is recovered as the steady-state currents vanish. Away from equilibrium, the correction terms responsible for the violation of the FDT, upon integration, are determined by a quantity characterizing the irreversibility of the steady state. The Harada–Sasa-type relation complements the equilibrium FDT by relating the violation of the latter to dissipation in nonequilibrium steady states.

VI. EXAMPLES

In this section, we illustrate three complementary aspects of the frequency-domain FRR. First, in Markov jump networks, the relation provides an exact edge-resolved decomposition of the covariance spectrum, revealing which transition channels dominate fluctuations at a given frequency. Second, in a driven diffusive system, the frequency-domain response bounds show that different uncertainty relations become relevant in different spectral regimes. Third, in a linear Langevin system, the frequency-domain TUR can be analyzed in a controlled setting, where its spectral structure and asymptotic limits can be examined explicitly.

A. Edge-resolved spectral decomposition in Markov jump networks

A distinctive feature of the frequency-domain FRR for Markov jump systems is the exact decomposition of the covariance spectrum into contributions from individual edges. For a single observable $\theta(t)$, we rewrite (84) as

$$C_{\theta,\theta}(\omega)=\sum_{n>m}C^{(nm)}_{\theta,\theta}(\omega), \tag{128}$$

with $C^{(nm)}_{\theta,\theta}(\omega)=|R^\theta_{\phi_{nm}}(\omega)|^2/A^\phi_{nm}$ denoting the contribution from the edge $m\leftrightarrow n$. Because this decomposition is frequency resolved, it identifies not only the dominant transitions on average, but also those that govern the dynamics within a given spectral window.

We first consider a unicyclic network,

$$E_1\underset{k_2^-}{\overset{k_1^+}{\rightleftarrows}}E_2\underset{k_3^-}{\overset{k_2^+}{\rightleftarrows}}E_3\cdots E_{N-1}\underset{k_N^-}{\overset{k_{N-1}^+}{\rightleftarrows}}E_N\underset{k_1^-}{\overset{k_N^+}{\rightleftarrows}}E_1, \tag{129}$$

with uniform forward and backward rates

$$k_i^+=ke^{\mathcal{F}/N},\qquad k_i^-=k, \tag{130}$$

where $\mathcal{F}$ is the cycle affinity. We consider both a state-dependent observable, $\theta(t)=\eta_1(t)$, and a current-like observable, $\theta(t)=\jmath_{21}(t)$. The corresponding edgewise decompositions are shown in Fig. 2. In both cases, the covariance spectrum exhibits a peak near the characteristic frequency set by the steady-state edge current

$$\omega^*=2\pi j_{\rm ss}=\frac{2\pi k}{N}\big(e^{\mathcal{F}/N}-1\big). \tag{131}$$

The decomposition shows that the first edge provides the dominant contribution over a broad frequency range. This dominance is particularly pronounced near the spectral peak for the state-dependent observable [Fig. 2(a,c,e,g)], whereas for the current-like observable [Fig. 2(b,d,f,h)] the contributions are more evenly distributed across edges. We observe that increasing the

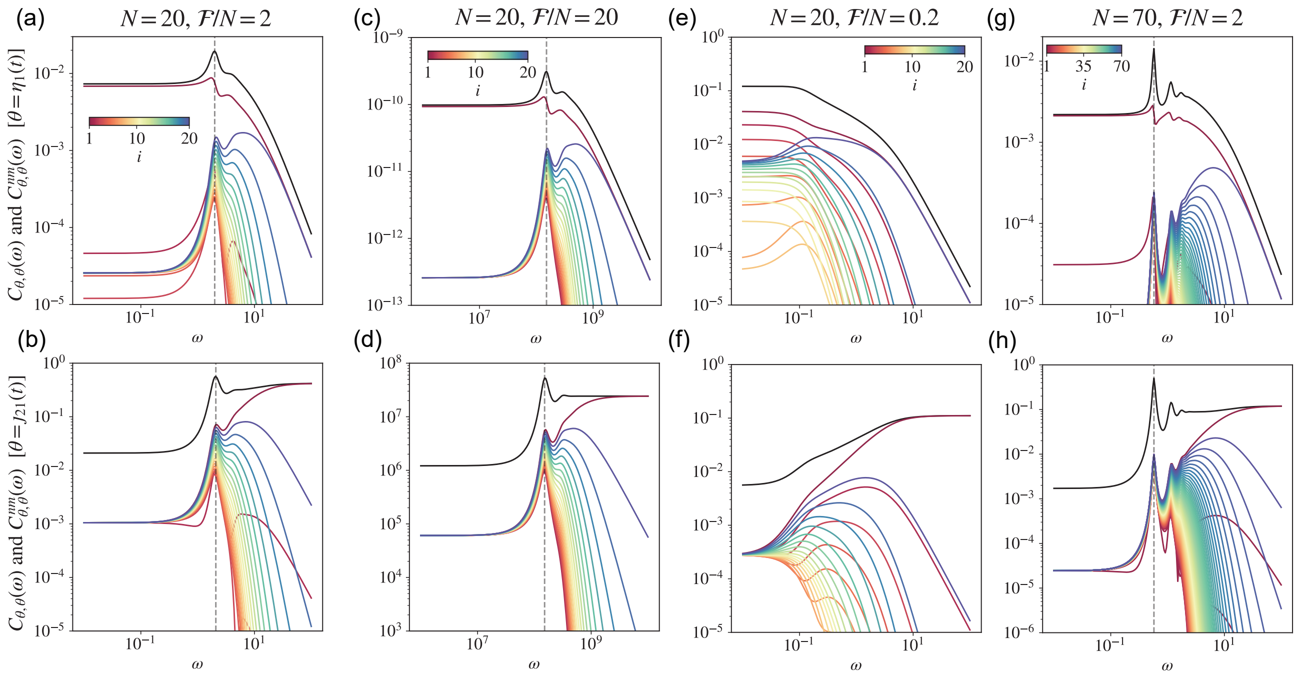

FIG. 2. Illustration of the frequency-domain FRR for a unicyclic network [Eq. (129)] for (a,c,e,g) state-dependent observable $\eta_1(t)$ and for (b,d,f,h) current-like observable $\jmath_{21}(t)$. Black lines denote the total fluctuation spectrum $C_{\theta,\theta}(\omega)$ and colored lines represent the edge-wise contributions $C^{nm}_{\theta,\theta}(\omega)$. Colors indicate the edge index, as shown by the color bar in panel (a). For example, $i = 8$ corresponds to the edge connecting E_8 and E_9. In panels (a-d) and (g,h), gray dotted vertical lines indicate the frequency at which $C_{\theta,\theta}(\omega)$ is maximized. Parameters: $k = 1$ for all panels. (a-f) $N = 20$, (g,h) $N = 70$. (a,b,g,h) $\mathcal{F}/N = 2$, (c,d) $\mathcal{F}/N = 20$, (e,f) $\mathcal{F}/N = 0.2$

affinity [Fig. 2(c,d)] or the number of states [Fig. 2(g,h)] sharpens the spectral peak, while decreasing the affinity suppresses it [Fig. 2(e,f)]. In all cases, the first edge remains the dominant contributor.

This example illustrates the utility of the frequency-domain FRR. A conventional covariance spectrum reveals a characteristic frequency of the dynamics, but does not indicate which transition channels are primarily responsible. By contrast, the decomposition (128) resolves the spectrum into contributions from individual edges, providing a direct view of the underlying network dynamics.

We next consider a simplified model of KaiC phosphorylation, shown in Fig. 3(a) [49, 50], which captures the core phosphorylation cycle of the cyanobacterial circadian clock. The network consists of 14 states, with K_i and $\bar{K}_i$ denoting the active and inactive KaiC states with i phosphorylations. As an observable, we consider the phosphorylation level

$$P(t) = \sum_i i\big[\eta_{K_i}(t) + \eta_{\bar{K}_i}(t)\big]. \tag{132}$$

The covariance spectrum $C_{P,P}(\omega)$, shown as the black curve in Fig. 3(b–d), exhibits a clear peak, reflecting the oscillatory dynamics of the phosphorylation process. The edge-resolved decomposition reveals a more detailed picture. At low frequency, the dominant contributions arise from the edges connecting the entry points of the daytime and nighttime branches to their neighboring states. Toward higher frequencies, the contributions from different edges become more comparable. Moreover, as shown in Fig. 3(d), the contributions from edges linking the day and night branches are approximately symmetric with respect to the triply phosphorylated state, while transitions involving the unphosphorylated and fully phosphorylated states contribute most strongly.

In a biochemical oscillator such as KaiC, the existence of a spectral peak alone does not reveal which part of the cycle controls the oscillation. The frequency-domain FRR addresses this limitation by assigning a quantitative contribution to each transition channel. This provides an operational interpretation of the spectrum: modifying a subset of transitions primarily affects the frequency range where they contribute most.

B. Frequency-dependent response bounds in a tilted periodic potential

We next illustrate that the uncertainty relations arising from the frequency-domain FRR are not merely formal extensions of static bounds, but provide frequency-dependent constraints on measurable response. To this

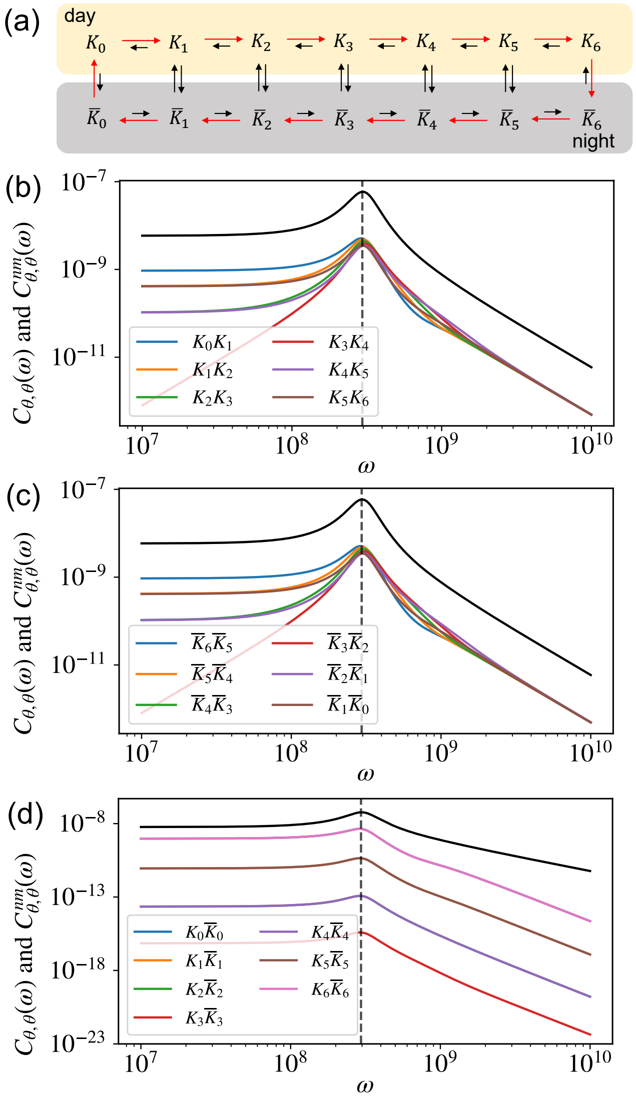

FIG. 3. Illustration of the frequency-domain FRR in the KaiC network. (a) KaiC cycle with 14 states. K_i and $\bar{K}_i$ denote the active and inactive states with i phosphates, respectively. (b-d) Contributions of individual edges to the FRR. In each panel, black lines denote the total fluctuation spectrum $C_{\theta,\theta}(\omega)$ of the phosphorylation level $P(t)$, while colored lines denote the contribution from each edge $C^{nm}_{\theta}(\omega)$. (b) Contributions from edges between day states. (c) Contributions from edges between night states. (d) Contributions from edges linking day and night states.

end, we consider an overdamped particle in a tilted periodic potential, shown in Fig. 4. This model is a standard setting for nonequilibrium transport and giant diffusion [51–54].

The dynamics is described by

$$\dot{x}(t) = \mu\big[f_0 - U'(x(t))\big] + \sqrt{2\mu T}\,\xi(t), \tag{133}$$

where μ is the mobility, T is the temperature, f_0 is the constant driving force, and $\xi(t)$ is Gaussian white noise satisfying

$$\langle \xi(t)\rangle = 0, \qquad \langle \xi(t)\xi(t')\rangle = \delta(t-t'). \tag{134}$$

The periodic potential is taken to be

$$U(x) = U_0 \cos\left(\frac{2\pi x}{L}\right), \tag{135}$$

with amplitude U_0 and period L. The observable is the instantaneous velocity, $\dot{x}(t)$.

The covariance spectrum $C_{\dot{x},\dot{x}}(\omega)$ and the response $R^{\dot{x}}_{f_0\mapsto f_0+\epsilon}(\omega)$ are shown in Fig. 4(a,b). These results show that both the response and fluctuations have a nontrivial frequency dependence, highlighting the importance of the frequency-domain viewpoint even in this simple driven diffusive model.

We first consider the frequency-domain response KUR associated with perturbing the driving force f_0. A homogeneous force perturbation with $\psi(x,t) = 1$ reduces (93)

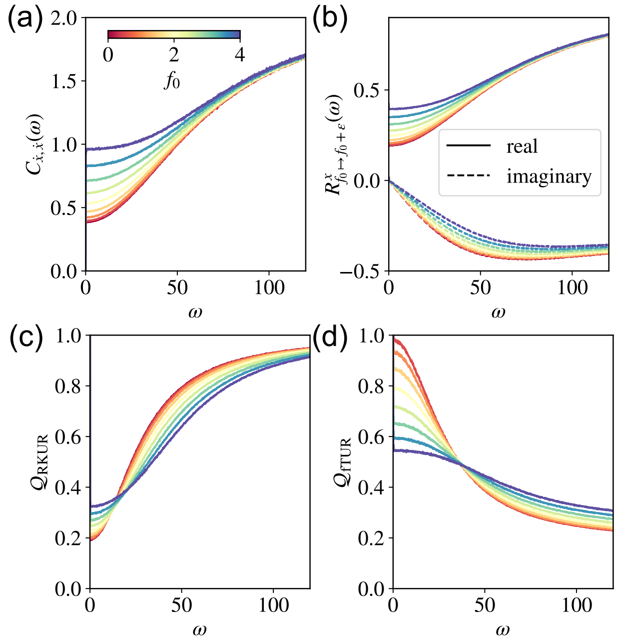

FIG. 4. A numerical illustration of the frequency-domain RKUR and TUR for a particle in a tilted potential. (a) Fourier transform of the velocity autocorrelation function. (b) Real (solid) and imaginary (dotted) parts of the Fourier-transformed response function. (c) Quality factor of the frequency-domain RKUR. (d) Quality factor of the frequency-domain TUR. In each panel, lines of different colors correspond to different values of f_0, as indicated by the color map in (a). Parameters: $\mu = 1$, $T = 1$, $U_0 = 2$, and $L = 2\pi$. Simulations are performed using the Euler–Maruyama method to integrate Eq. (133), with time step $dt = 0.001$, maximum time $t_{\max} = 50$, and ensemble size $N_{\rm ens} = 10^5$.

to

$$C_{\dot{x},\dot{x}}(\omega) \geq \frac{2T}{\mu}\left|R^{\dot{x}}_{f_0\mapsto f_0+\epsilon}(\omega)\right|^2. \tag{136}$$

To quantify the tightness of this inequality, we define a quality factor

$$\mathcal{Q}_{\mathrm{RKUR}}(\omega) = \frac{2T}{\mu}\frac{|R^{\dot{x}}_{f_0\mapsto f_0+\epsilon}(\omega)|^2}{C_{\dot{x},\dot{x}}(\omega)}. \tag{137}$$

The behavior of $\mathcal{Q}_{\mathrm{RKUR}}(\omega)$ is shown in Fig. 4(c). In this model, the quality factor increases monotonically with ω and saturates at high frequency. This trend reflects that the bound becomes tighter at higher frequencies, where the velocity response is dominated by the short-time effect of the force perturbation, before the dynamics explores multiple periods of the tilted potential.

We compare the response KUR with the frequency-domain TUR shown in Fig. 4(d). Perturbing $\ln\mu$ yields the frequency-domain response TUR, which coincides with the frequency-domain TUR for the velocity observable in this model. The corresponding bound can be written as

$$C_{\dot{x},\dot{x}}(\omega) \geq \frac{2\langle\dot{x}\rangle_{\mathrm{ss}}^2}{\sigma}, \tag{138}$$

where σ is the steady-state entropy production rate. We define the associated quality factor by

$$\mathcal{Q}_{\mathrm{fTUR}}(\omega) = \frac{2\langle\dot{x}\rangle_{\mathrm{ss}}^2}{\sigma\, C_{\dot{x},\dot{x}}(\omega)}. \tag{139}$$

As shown in Fig. 4(d), $\mathcal{Q}_{\mathrm{fTUR}}(\omega)$ decreases monotonically with ω, in contrast to $\mathcal{Q}_{\mathrm{RKUR}}(\omega)$, and is tightest in the static limit $\omega \to 0$.

The contrast between Fig. 4(c) and (d) highlights a key aspect of this example. The two bounds constrain different physical quantities. Equation (136) constrains the response of the velocity to a perturbation of the driving force, whereas Eq. (138) constrains the steady-state drift relative to fluctuations. It is therefore natural that the two quality factors are tight in different spectral regimes. In this model, the force-response bound becomes tighter toward higher frequencies, while the thermodynamic bound is strongest at low frequency, where steady-state drift dominates the spectrum.

From an experimental perspective, this example is particularly relevant, as both the velocity spectrum and the force response are directly accessible. Figure 4 thus goes beyond a model-specific numerical check, revealing how different uncertainty bounds become tight in distinct spectral regimes and thereby probe different aspects of the dynamics. The frequency-domain FRR and its resulting bounds thus provide a practical framework for interpreting response and fluctuation data in driven diffusive systems.

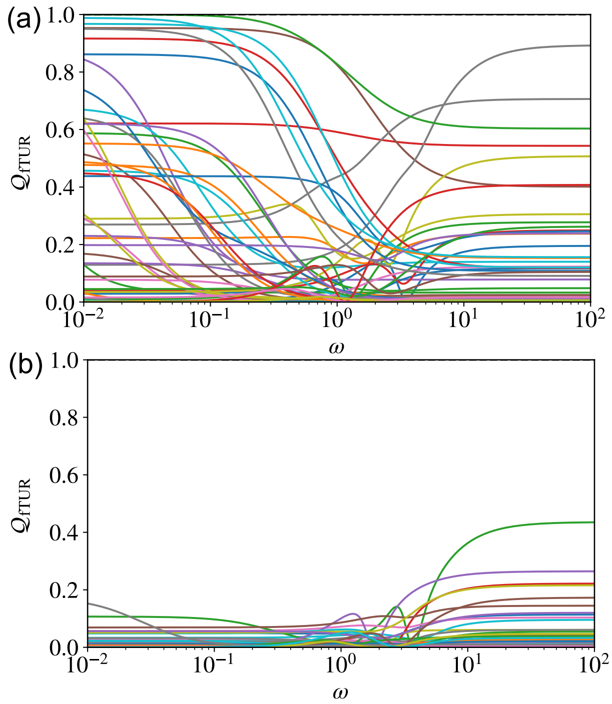

FIG. 5. A numerical illustration of Eq. (142) for the linear Langevin system [Eq. (140)] for dimensions (a) $N = 2$ and (b) $N = 4$. Elements of A are sampled from unit Gaussian distribution, while discarding realizations for which any eigenvalue is non-positive. The matrix B is diagonal with entries $\sqrt{2T}$, where T is sampled uniformly from $[1, 5]$. Elements of W are sampled from a unit Gaussian distribution. For each panel, 50 independent realizations are shown.

C. Frequency-domain TUR in a linear Langevin system

We finally consider a linear Langevin system, for which all analytical expressions involved in the frequency-domain TUR are available. This example clarifies the structure of the frequency-domain TUR and show explicitly how the bound connects the low- and high-frequency regimes.

The dynamics is described by

$$\dot{\boldsymbol{x}}(t) = -A\boldsymbol{x}(t) + B\boldsymbol{\xi}(t), \tag{140}$$

where A is a stable drift matrix, B is a constant noise-amplitude matrix, and $\boldsymbol{\xi}(t)$ is Gaussian white noise with zero mean and unit covariance. We consider the current-like observable

$$\theta(t) = \boldsymbol{x}(t)^{\mathsf{T}} W \circ \dot{\boldsymbol{x}}(t), \tag{141}$$

where W is an antisymmetric matrix. For this observable, the frequency-domain TUR (98) reduces to

$$\frac{2\langle\theta\rangle_{\rm ss}^2}{\sigma\, C_{\theta,\theta}(\omega)} \leq 1, \tag{142}$$

with σ denoting the steady-state entropy production rate. The corresponding quality factor is

$$\mathcal{Q}_{\rm fTUR} = \frac{2\langle\theta\rangle_{\rm ss}^2}{\sigma\, C_{\theta,\theta}(\omega)}. \tag{143}$$

The behavior of $\mathcal{Q}_{\rm fTUR}$ is shown in Fig. 5. A first notable feature is its generally nonmonotonic dependence on frequency. Even in a linear system, the frequency-domain TUR is therefore not characterized by a single preferred spectral regime. Instead, its tightness depends on the interplay between deterministic relaxation, noise, and the observable defined by the matrix W. A second feature is that the quality factor decreases with increasing system dimension N, indicating that the bound is typically looser in higher-dimensional linear dynamics. This trend is visible in the comparison between Fig. 5(a) and (b).

The linear setting makes the asymptotic content of the frequency-domain TUR transparent. In the limit $\omega \to 0$, Eq. (142) reduces to the conventional long-time TUR [11], while in the limit $\omega \to \infty$ it approaches the bound known as the entropic bound [55]. The frequency-domain TUR thus provides a single relation that interpolates continuously between these two limiting thermodynamic constraints. Figure 5 illustrates this interpolation in a setting where both the covariance spectrum and entropy production rate are analytically tractable.

In this linear example, both the covariance spectrum and the entropy production rate can be computed analytically, allowing the limiting behavior of the frequency-domain TUR to be examined explicitly. In the limit $\omega \to 0$, the frequency-domain TUR (142) reduces to the conventional long-time TUR [11], while in the limit $\omega \to \infty$ it recovers the entropic bound derived in [55]. The frequency-domain TUR thus provides a single relation that interpolates continuously between these two limiting thermodynamic constraints. This crossover is shown in Fig. 5.

VII. CONCLUSION

In this work, we have developed a fluctuation–response theory in the frequency domain for nonequilibrium steady states. The central result is a frequency-domain FRR that expresses the power spectrum of general observables in terms of local linear responses at the same frequency. We have established this relation for both overdamped Langevin and Markov jump systems. The decomposition is formulated in configuration space in the Langevin case, while in the Markov jump case it is over transition edges.

The relation applies to state-dependent observables, current-like observables, and their combinations. It thus provides a unified framework for describing fluctuations of occupations and currents in continuous and discrete stochastic dynamics. Compared with earlier nonequilibrium FRRs formulated mainly for static or long-time covariances [30, 34], the present formulation applies directly at finite frequency.

We have further shown that several consequences follow from the frequency-domain FRR. By applying the Cauchy–Schwarz inequality, we have obtained frequency-domain RURs, which reduce to KUR and TUR for specific perturbations. In the equilibrium limit, the FRR recovers the FDT, while away from equilibrium the remaining current-dependent terms yield Harada–Sasa-type relations. These results show that these seemingly different relations arise as different consequences of a single underlying frequency-domain fluctuation–response structure.

The examples illustrate complementary aspects of the theory. For Markov jump networks, the edge-resolved form of the relation decomposes the power spectrum into contributions from individual transition channels. For driven Langevin systems, the frequency-dependent bounds show that different perturbation classes are relevant in different spectral regimes. These examples demonstrate how the theory serves not only as a formal identity but also as a practical tool for analyzing frequency-resolved fluctuation and response spectra.

Several directions remain open. First, the present formulation suggests an experimental route for reconstructing fluctuation spectra from local or controlled finite-frequency responses, especially in systems where direct spectral measurements and perturbative measurements are both accessible. Second, extending the exact frequency-domain relation to underdamped Langevin dynamics would broaden its applicability to inertial stochastic systems and molecular-scale transport. Third, it would be interesting to investigate whether analogous frequency-domain fluctuation–response structures can be formulated for open quantum systems, where response, noise, and dissipation are constrained by both stochastic and quantum effects.

Several directions remain open. First, an important direction is to test experimentally whether fluctuation spectra can be reconstructed from local or controlled finite-frequency responses, particularly in systems where both spectral and perturbative measurements are accessible. Second, extending the frequency-domain FRR to underdamped Langevin dynamics would broaden its applicability to inertial stochastic systems. Third, it is natural to ask whether analogous frequency-domain fluctuation–response structures can be formulated for open quantum systems, where response, noise, and dissipation are constrained by both stochastic and quantum effects.

Acknowledgements.– This research was supported by NRF Grants No. 2017R1D1A1B06035497 (H.P.) and individual KIAS Grants No. PG064902 (J.S.L.), PG089402 (H.-M.C.), QP013602 (H.P.), and QP10301 (E.K.) at the

Korea Institute for Advanced Study.

Appendix A: Technical details for overdamped Langevin systems

1. Perturbed Fokker–Planck generator and local response formulas

In this subsection, we derive the local response formulas stated in Sec. III. We consider the overdamped Langevin dynamics

$$\dot{\boldsymbol{x}}(t) = M(\boldsymbol{x}(t))\boldsymbol{F}(\boldsymbol{x}(t)) + \sqrt{2}\,B(\boldsymbol{x}(t)) \circledast \boldsymbol{\xi}(t), \qquad \text{(A1)}$$

where $\circledast$ denotes the anti-Itô product, and $\hat{\mathcal{L}}_{\boldsymbol{x}}$ is the Fokker–Planck generator given by

$$\hat{\mathcal{L}}_{\boldsymbol{x}} = -\nabla_{\boldsymbol{x}}^{\mathsf{T}}\hat{\mathcal{J}}_{\boldsymbol{x}}, \qquad \hat{\mathcal{J}}_{\boldsymbol{x}} = M(\boldsymbol{x})\big[\boldsymbol{F}(\boldsymbol{x}) - T(\boldsymbol{x})\nabla_{\boldsymbol{x}}\big], \quad \text{(A2)}$$

We use the relation $\frac{1}{2}B(\boldsymbol{x})B(\boldsymbol{x})^{\mathsf{T}} = D(\boldsymbol{x}) = M(\boldsymbol{x})T(\boldsymbol{x})$. The steady-state distribution $\pi(\boldsymbol{x})$ satisfies

$$\hat{\mathcal{L}}_{\boldsymbol{x}}\pi(\boldsymbol{x}) = 0, \qquad \text{(A3)}$$

and the corresponding steady-state current is

$$\boldsymbol{j}_{\rm ss}(\boldsymbol{x}) = \hat{\mathcal{J}}_{\boldsymbol{x}}\pi(\boldsymbol{x}). \qquad \text{(A4)}$$

We consider a local perturbation of the kth component of $\phi \in \{\boldsymbol{F}, \ln M, T\}$ at the point $\boldsymbol{z}$ and time $t=0$:

$$\phi_k(\boldsymbol{x}) \mapsto \phi_k(\boldsymbol{x}) + \epsilon\,\delta(\boldsymbol{x}-\boldsymbol{z})\delta(t). \qquad \text{(A5)}$$

At the level of the Fokker–Planck generator, the perturbation can be written as

$$\hat{\mathcal{L}}_{\boldsymbol{x}} \mapsto \hat{\mathcal{L}}_{\boldsymbol{x}} - \epsilon\,\delta(t)\nabla_{\boldsymbol{x}}^{\mathsf{T}}\delta(\boldsymbol{x}-\boldsymbol{z})\,\hat{\mathcal{K}}_{\phi_k,\boldsymbol{x}}\,, \qquad \text{(A6)}$$

where $\hat{\mathcal{K}}_{\phi_k,\boldsymbol{x}}$ depends on the perturbed quantity. In the diagonal setting adopted in the main text, these operators are

$$\hat{\mathcal{K}}_{F_k,\boldsymbol{x}} = M(\boldsymbol{x})\,\boldsymbol{e}_k, \qquad \text{(A7)}$$

$$\hat{\mathcal{K}}_{\ln M_k,\boldsymbol{x}} = \mu_k(\boldsymbol{x})\,\boldsymbol{e}_k\boldsymbol{e}_k^{\mathsf{T}}\big[\boldsymbol{F}(\boldsymbol{x}) - T(\boldsymbol{x})\nabla_{\boldsymbol{x}}\big], \qquad \text{(A8)}$$

and

$$\hat{\mathcal{K}}_{T_k,\boldsymbol{x}} = -M(\boldsymbol{x})\,\boldsymbol{e}_k\boldsymbol{e}_k^{\mathsf{T}}\nabla_{\boldsymbol{x}}. \qquad \text{(A9)}$$

Here $\boldsymbol{e}_k$ denotes the kth unit vector.

Assuming a steady-state initial condition, we expand the probability density as

$$p(\boldsymbol{x},t) = \pi(\boldsymbol{x}) + \epsilon\,q_{\phi_k}(\boldsymbol{x},t;\boldsymbol{z}) + O(\epsilon^2). \qquad \text{(A10)}$$

Substituting this expansion into the perturbed Fokker–Planck equation and retaining terms up to linear order in ϵ, we obtain

$$\partial_t q_{\phi_k}(\boldsymbol{x},t;\boldsymbol{z}) = \hat{\mathcal{L}}_{\boldsymbol{x}} q_{\phi_k}(\boldsymbol{x},t;\boldsymbol{z}) - \nabla_{\boldsymbol{x}}^{\mathsf{T}}\delta(\boldsymbol{x}-\boldsymbol{z})\,\hat{\mathcal{K}}_{\phi_k,\boldsymbol{z}}\pi(\boldsymbol{z})\,\delta(t). \qquad \text{(A11)}$$

It is therefore natural to define

$$N_{\phi_k}(\boldsymbol{z}) \equiv \hat{\mathcal{K}}_{\phi_k,\boldsymbol{z}}\pi(\boldsymbol{z}). \qquad \text{(A12)}$$

With this notation, the linearized equation becomes

$$\partial_t q_{\phi_k}(\boldsymbol{x},t;\boldsymbol{z}) = \hat{\mathcal{L}}_{\boldsymbol{x}} q_{\phi_k}(\boldsymbol{x},t;\boldsymbol{z}) - \delta(t)\nabla_{\boldsymbol{x}}^{\mathsf{T}}\delta(\boldsymbol{x}-\boldsymbol{z})\,N_{\phi_k}(\boldsymbol{z})\,. \qquad \text{(A13)}$$

Solving the linearized equation by convolution with the unperturbed propagator $P(\boldsymbol{x},t|\boldsymbol{z},0)$, we obtain

$$q_{\phi_k}(\boldsymbol{x},t;\boldsymbol{z}) = \big[N_{\phi_k}(\boldsymbol{z})\big]^{\mathsf{T}}\nabla_{\boldsymbol{z}}P(\boldsymbol{x},t|\boldsymbol{z},0), \qquad \text{(A14)}$$

where the derivative with respect to $\boldsymbol{z}$ arises from integration by parts acting on the delta function. Introducing the excess propagator

$$H(\boldsymbol{x},\boldsymbol{z};\omega) = \int_0^\infty \big[P(\boldsymbol{x},t|\boldsymbol{z},0) - \pi(\boldsymbol{x})\big]e^{i\omega t}\,dt, \qquad \text{(A15)}$$

the response of the empirical density is given by

$$R^{\rho(\boldsymbol{x})}_{\phi_k(\boldsymbol{z})}(\omega) = \big[N_{\phi_k}(\boldsymbol{z})\big]^{\mathsf{T}}\nabla_{\boldsymbol{z}}H(\boldsymbol{x},\boldsymbol{z};\omega). \qquad \text{(A16)}$$

The response of the empirical current follows from the linear relation $\boldsymbol{\jmath}(\boldsymbol{x},t) = \hat{\mathcal{J}}_{\boldsymbol{x}}p(\boldsymbol{x},t)$:

$$\delta\langle\boldsymbol{\jmath}(\boldsymbol{x},t)\rangle = \delta(\boldsymbol{x}-\boldsymbol{z})\,N_{\phi_k}(\boldsymbol{z})\,\delta(t) + \hat{\mathcal{J}}_{\boldsymbol{x}}\,q_{\phi_k}(\boldsymbol{x},t;\boldsymbol{z}), \qquad \text{(A17)}$$

where the first and second terms arise from the perturbations of $\hat{\mathcal{J}}_{\boldsymbol{x}}$ and $p(\boldsymbol{x},t)$, respectively. Taking the Fourier transform in time, we obtain

$$R^{\boldsymbol{\jmath}(\boldsymbol{x})}_{\phi_k(\boldsymbol{z})}(\omega) = \mathcal{P}(\boldsymbol{x},\boldsymbol{z};\omega)\,N_{\phi_k}(\boldsymbol{z}). \qquad \text{(A18)}$$

where

$$\mathcal{P}(\boldsymbol{x},\boldsymbol{z};\omega) = I\,\delta(\boldsymbol{x}-\boldsymbol{z}) + \hat{\mathcal{J}}_{\boldsymbol{x}}\nabla_{\boldsymbol{z}}^{\mathsf{T}}H(\boldsymbol{x},\boldsymbol{z};\omega). \qquad \text{(A19)}$$

Finally, in the diagonal setting adopted in the main text, the explicit local prefactors are given by

$$N_{F_k}(\boldsymbol{z}) = \pi(\boldsymbol{z})\mu_k(\boldsymbol{z})\,\boldsymbol{e}_k, \qquad \text{(A20)}$$

$$N_{\ln M_k}(\boldsymbol{z}) = j_k^{\rm ss}(\boldsymbol{z})\,\boldsymbol{e}_k, \qquad \text{(A21)}$$

and

$$N_{T_k}(\boldsymbol{z}) = -\mu_k(\boldsymbol{z})\,\partial_{z_k}\pi(\boldsymbol{z})\,\boldsymbol{e}_k. \qquad \text{(A22)}$$

The second identity follows from the definition of the steady-state current,

$$j_k^{\rm ss}(\boldsymbol{z}) = \mu_k(\boldsymbol{z})\Big[F_k(\boldsymbol{z})\pi(\boldsymbol{z}) - T_k(\boldsymbol{z})\partial_{z_k}\pi(\boldsymbol{z})\Big]. \qquad \text{(A23)}$$

Thus, once the perturbation-dependent vector $N_{\phi_k}(\boldsymbol{z})$ is identified, both density and current responses are determined by the same excess propagator.

2. Properties of the excess propagator

In this subsection, we derive the identities for the excess propagator used in Sec. III. We recall its definition,

$$H(\boldsymbol{x},\boldsymbol{z};\omega) = \int_0^\infty \big[P(\boldsymbol{x},t|\boldsymbol{z},0) - \pi(\boldsymbol{x})\big] e^{i\omega t}\, dt. \quad \text{(A24)}$$

The propagator satisfies both the forward and backward Fokker–Planck equations,

$$\partial_t P(\boldsymbol{x},t|\boldsymbol{z},0) = \hat{\mathcal{L}}_{\boldsymbol{x}} P(\boldsymbol{x},t|\boldsymbol{z},0), \quad \text{(A25)}$$

$$\partial_t P(\boldsymbol{x},t|\boldsymbol{z},0) = \hat{\mathcal{L}}_{\boldsymbol{z}}^\dagger P(\boldsymbol{x},t|\boldsymbol{z},0), \quad \text{(A26)}$$

together with

$$\lim_{t\to 0^+} P(\boldsymbol{x},t|\boldsymbol{z},0) = \delta(\boldsymbol{x}-\boldsymbol{z}), \qquad \lim_{t\to\infty} P(\boldsymbol{x},t|\boldsymbol{z},0) = \pi(\boldsymbol{x}), \quad \text{(A27)}$$

where $\hat{\mathcal{L}}_{\boldsymbol{z}}^\dagger$ denotes the adjoint of the Fokker-Planck generator acting the initial position $\boldsymbol{z}$.

We first show that

$$\int d\boldsymbol{z}\, H(\boldsymbol{x},\boldsymbol{z};\omega)\pi(\boldsymbol{z}) = 0. \quad \text{(A28)}$$

Using the stationarity of the steady-state distribution,

$$\int d\boldsymbol{z}\, P(\boldsymbol{x},t|\boldsymbol{z},0)\pi(\boldsymbol{z}) = \pi(\boldsymbol{x}), \quad \text{(A29)}$$

and therefore

$$\begin{aligned}&\int d\boldsymbol{z}\, H(\boldsymbol{x},\boldsymbol{z};\omega)\pi(\boldsymbol{z}) \\ &= \int_0^\infty dt\, e^{i\omega t} \int d\boldsymbol{z}\, \big[P(\boldsymbol{x},t|\boldsymbol{z},0) - \pi(\boldsymbol{x})\big]\pi(\boldsymbol{z}) \\ &= 0.\end{aligned} \quad \text{(A30)}$$

We next show that

$$(i\omega + \hat{\mathcal{L}}_{\boldsymbol{x}}) H(\boldsymbol{x},\boldsymbol{z};\omega) = -\delta(\boldsymbol{x}-\boldsymbol{z}) + \pi(\boldsymbol{x}). \quad \text{(A31)}$$

This follows by rewriting the integrand as a total time derivative and evaluating the boundary terms at $t=0$ and $t\to\infty$:

$$\begin{aligned}&(i\omega + \hat{\mathcal{L}}_{\boldsymbol{x}}) H(\boldsymbol{x},\boldsymbol{z};\omega) \\ &= \int_0^\infty dt\, e^{i\omega t}\Big[i\omega\big(P(\boldsymbol{x},t|\boldsymbol{z},0) - \pi(\boldsymbol{x})\big) + \hat{\mathcal{L}}_{\boldsymbol{x}} P(\boldsymbol{x},t|\boldsymbol{z},0)\Big] \\ &= \int_0^\infty dt\, \partial_t \Big(e^{i\omega t}[P(\boldsymbol{x},t|\boldsymbol{z},0) - \pi(\boldsymbol{x})]\Big) \\ &= \Big[e^{i\omega t}[P(\boldsymbol{x},t|\boldsymbol{z},0) - \pi(\boldsymbol{x})]\Big]_{t=0}^{t=\infty} \\ &= -\delta(\boldsymbol{x}-\boldsymbol{z}) + \pi(\boldsymbol{x}).\end{aligned} \quad \text{(A32)}$$

Similarly,

$$(i\omega + \hat{\mathcal{L}}_{\boldsymbol{z}}^\dagger) H(\boldsymbol{x},\boldsymbol{z};\omega) = -\delta(\boldsymbol{x}-\boldsymbol{z}) + \pi(\boldsymbol{x}). \quad \text{(A33)}$$

This follows by the same argument, using the backward Fokker–Planck equation.

Equations (A31) and (A33) imply that $H(\boldsymbol{x},\boldsymbol{z};\omega)$ is the resolvent of the Fokker–Planck operator projected onto the subspace orthogonal to the steady state.

3. Covariances of empirical density and current

We now derive the covariance formulas for the empirical density and current. We begin with

$$\rho(\boldsymbol{x},t) = \delta(\boldsymbol{x} - \boldsymbol{x}(t)). \quad \text{(A34)}$$

For $t>0$, the connected two-time correlation is given by

$$\langle \rho(\boldsymbol{x},t)\rho(\boldsymbol{y},0)\rangle - \pi(\boldsymbol{x})\pi(\boldsymbol{y}) = \big[P(\boldsymbol{x},t|\boldsymbol{y},0) - \pi(\boldsymbol{x})\big]\pi(\boldsymbol{y}), \quad \text{(A35)}$$

whereas for $t<0$,

$$\langle \rho(\boldsymbol{x},t)\rho(\boldsymbol{y},0)\rangle - \pi(\boldsymbol{x})\pi(\boldsymbol{y}) = \big[P(\boldsymbol{y},-t|\boldsymbol{x},0) - \pi(\boldsymbol{y})\big]\pi(\boldsymbol{x}), \quad \text{(A36)}$$

which follows from time-translation invariance, $P(\boldsymbol{y},0|\boldsymbol{x},t) = P(\boldsymbol{y},-t|\boldsymbol{x},0)$. Substituting these expressions into the definition of the covariance spectrum (1) gives

$$C_{\rho(\boldsymbol{x}),\rho(\boldsymbol{y})}(\omega) = H(\boldsymbol{x},\boldsymbol{y};\omega)\pi(\boldsymbol{y}) + H(\boldsymbol{y},\boldsymbol{x};-\omega)\pi(\boldsymbol{x}). \quad \text{(A37)}$$

As shown in the next subsection, this can be equivalently expressed in the quadratic form

$$\begin{aligned}&C_{\rho(\boldsymbol{x}),\rho(\boldsymbol{y})}(\omega) \\ &= 2\int d\boldsymbol{z}\, \pi(\boldsymbol{z})\, \big[\nabla_{\boldsymbol{z}} H(\boldsymbol{x},\boldsymbol{z};\omega)\big]^\mathsf{T} D(\boldsymbol{z}) \nabla_{\boldsymbol{z}} H(\boldsymbol{y},\boldsymbol{z};-\omega).\end{aligned} \quad \text{(A38)}$$

We next decompose the empirical current into drift and fluctuation contributions as

$$\boldsymbol{\jmath}(\boldsymbol{x},t) = \hat{\mathcal{J}}_{\boldsymbol{x}} \rho(\boldsymbol{x},t) + \boldsymbol{\zeta}(\boldsymbol{x},t), \quad \text{(A39)}$$

where

$$\boldsymbol{\zeta}(\boldsymbol{x},t)=\boldsymbol{\eta}(t)\,\delta(\boldsymbol{x}-\boldsymbol{x}(t)),\qquad \boldsymbol{\eta}(t)=\sqrt{2}\,B(\boldsymbol{x}(t))\bullet\boldsymbol{\xi}(t). \tag{A40}$$

In the steady state, the noise term has covariance

$$\langle\zeta_i(\boldsymbol{x},t)\zeta_j(\boldsymbol{y},t')\rangle=2\pi(\boldsymbol{x})D_{ij}(\boldsymbol{x})\delta(\boldsymbol{x}-\boldsymbol{y})\delta(t-t'), \tag{A41}$$

and therefore

$$C_{\boldsymbol{\zeta}(\boldsymbol{x}),\boldsymbol{\zeta}(\boldsymbol{y})^{\mathsf{T}}}(\omega)=2\pi(\boldsymbol{x})D(\boldsymbol{x})\delta(\boldsymbol{x}-\boldsymbol{y}). \tag{A42}$$

The mixed density–noise covariance is given by

$$C_{\rho(\boldsymbol{x}),\boldsymbol{\zeta}(\boldsymbol{y})^{\mathsf{T}}}(\omega)=2\pi(\boldsymbol{y})\nabla_{\boldsymbol{y}}^{\mathsf{T}}H(\boldsymbol{x},\boldsymbol{y};\omega)D(\boldsymbol{y}), \tag{A43}$$

which follows from the definition of $\boldsymbol{\zeta}$ and the delta-correlated noise. Similarly,

$$C_{\boldsymbol{\zeta}(\boldsymbol{x}),\rho(\boldsymbol{y})}(\omega)=2\pi(\boldsymbol{x})D(\boldsymbol{x})\nabla_{\boldsymbol{x}}H(\boldsymbol{y},\boldsymbol{x};-\omega). \tag{A44}$$

Using the decomposition (A39), the mixed density–current covariance is given by

$$C_{\rho(\boldsymbol{x}),\boldsymbol{J}(\boldsymbol{y})^{\mathsf{T}}}(\omega)=[\hat{\mathcal{J}}_{\boldsymbol{y}}C_{\rho(\boldsymbol{x}),\rho(\boldsymbol{y})}(\omega)]^{\mathsf{T}}+C_{\rho(\boldsymbol{x}),\boldsymbol{\zeta}(\boldsymbol{y})^{\mathsf{T}}}(\omega), \tag{A45}$$

while the current–current covariance is given by

$$\begin{aligned}C_{\boldsymbol{J}(\boldsymbol{x}),\boldsymbol{J}(\boldsymbol{y})^{\mathsf{T}}}(\omega)&=\hat{\mathcal{J}}_{\boldsymbol{x}}[\hat{\mathcal{J}}_{\boldsymbol{y}}C_{\rho(\boldsymbol{x}),\rho(\boldsymbol{y})}(\omega)]^{\mathsf{T}}+\hat{\mathcal{J}}_{\boldsymbol{x}}C_{\rho(\boldsymbol{x}),\boldsymbol{\zeta}(\boldsymbol{y})^{\mathsf{T}}}(\omega)\\&\quad+[\hat{\mathcal{J}}_{\boldsymbol{y}}C_{\boldsymbol{\zeta}(\boldsymbol{x}),\rho(\boldsymbol{y})}(\omega)]^{\mathsf{T}}+C_{\boldsymbol{\zeta}(\boldsymbol{x}),\boldsymbol{\zeta}(\boldsymbol{y})^{\mathsf{T}}}(\omega).\end{aligned} \tag{A46}$$

Substituting (A37), (A42), (A43), and (A44), together with the quadratic representation (A38), we obtain

$$C_{\rho(\boldsymbol{x}),\boldsymbol{J}(\boldsymbol{y})^{\mathsf{T}}}(\omega) \tag{A47}$$

$$=2\int d\boldsymbol{z}\,\pi(\boldsymbol{z})\,\nabla_{\boldsymbol{z}}^{\mathsf{T}}H(\boldsymbol{x},\boldsymbol{z};\omega)D(\boldsymbol{z})\,\big[\mathcal{P}(\boldsymbol{y},\boldsymbol{z};\omega)\big]^{\dagger}, \tag{A48}$$

and

$$C_{\boldsymbol{J}(\boldsymbol{x}),\boldsymbol{J}(\boldsymbol{y})^{\mathsf{T}}}(\omega)=2\int d\boldsymbol{z}\,\pi(\boldsymbol{z})\,\mathcal{P}(\boldsymbol{x},\boldsymbol{z};\omega)D(\boldsymbol{z})\,\big[\mathcal{P}(\boldsymbol{y},\boldsymbol{z};\omega)\big]^{\dagger}. \tag{A49}$$

4. Proof of the quadratic representation for the density–density covariance

In this subsection, we prove the quadratic representation (A38) of the density–density covariance. We first rewrite $H(\boldsymbol{x},\boldsymbol{y};\omega)\pi(\boldsymbol{y})$ in terms of a delta function to exploit the resolvent identity:

$$H(\boldsymbol{x},\boldsymbol{y};\omega)\pi(\boldsymbol{y})=\int d\boldsymbol{z}\,\pi(\boldsymbol{z})H(\boldsymbol{x},\boldsymbol{z};\omega)\delta(\boldsymbol{y}-\boldsymbol{z}). \tag{A50}$$

Using the identity (A33) we rewrite the delta function as

$$\delta(\boldsymbol{y}-\boldsymbol{z})=\pi(\boldsymbol{y})+i\omega H(\boldsymbol{y},\boldsymbol{z};-\omega)-\hat{\mathcal{L}}_{\boldsymbol{z}}^{\dagger}H(\boldsymbol{y},\boldsymbol{z};-\omega). \tag{A51}$$

Substituting (A51) into (A50), we have

$$\begin{aligned}H(\boldsymbol{x},\boldsymbol{y};\omega)\pi(\boldsymbol{y})&=i\omega\int d\boldsymbol{z}\,\pi(\boldsymbol{z})H(\boldsymbol{x},\boldsymbol{z};\omega)H(\boldsymbol{y},\boldsymbol{z};-\omega)\\&\quad-\int d\boldsymbol{z}\,\pi(\boldsymbol{z})H(\boldsymbol{x},\boldsymbol{z};\omega)\hat{\mathcal{L}}_{\boldsymbol{z}}^{\dagger}H(\boldsymbol{y},\boldsymbol{z};-\omega),\end{aligned} \tag{A52}$$

where the term proportional to $\pi(\boldsymbol{y})$ vanishes after integration over $\boldsymbol{z}$ due to the property (A28). Using $\hat{\mathcal{L}}_{\boldsymbol{z}}=-\nabla_{\boldsymbol{z}}^{\mathsf{T}}\hat{\mathcal{J}}_{\boldsymbol{z}}$ and integration by parts yields

$$\begin{aligned}&H(\boldsymbol{x},\boldsymbol{y};\omega)\pi(\boldsymbol{y})\\&=i\omega\int d\boldsymbol{z}\,\pi(\boldsymbol{z})H(\boldsymbol{x},\boldsymbol{z};\omega)H(\boldsymbol{y},\boldsymbol{z};-\omega)\\&\quad+\int d\boldsymbol{z}\,\pi(\boldsymbol{z})\nabla_{\boldsymbol{z}}^{\mathsf{T}}H(\boldsymbol{x},\boldsymbol{z};\omega)D(\boldsymbol{z})\nabla_{\boldsymbol{z}}H(\boldsymbol{y},\boldsymbol{z};-\omega)\\&\quad-\int d\boldsymbol{z}\,H(\boldsymbol{x},\boldsymbol{z};\omega)\,\big[\boldsymbol{j}_{\rm ss}(\boldsymbol{z})\big]^{\mathsf{T}}\nabla_{\boldsymbol{z}}H(\boldsymbol{y},\boldsymbol{z};-\omega).\end{aligned} \tag{A53}$$

Similarly, $H(\boldsymbol{y},\boldsymbol{x};-\omega)\pi(\boldsymbol{x})$ is obtained by exchanging $\boldsymbol{x}\leftrightarrow\boldsymbol{y}$ and $\omega\leftrightarrow-\omega$. Adding the two expressions, the first terms proportional to $i\omega$ cancel. The current-dependent terms (the third terms) combine into

$$\int d\boldsymbol{z}\,\big[\boldsymbol{j}_{\rm ss}(\boldsymbol{z})\big]^{\mathsf{T}}\nabla_{\boldsymbol{z}}\Big[H(\boldsymbol{x},\boldsymbol{z};\omega)H(\boldsymbol{y},\boldsymbol{z};-\omega)\Big], \tag{A54}$$

which vanishes since $\nabla_{\boldsymbol{z}}^{\mathsf{T}}\boldsymbol{j}_{\rm ss}(\boldsymbol{z})=0$ and the boundary contribution is zero. Recognizing that the remaining term is twice the second term of (A53) completes the proof of (A38).

5. Explicit forms of the perturbation weight matrices $A^{\phi}(\boldsymbol{z})$

In this subsection, we collect the explicit forms of the perturbation weight matrices $A^{\phi}(\boldsymbol{z})$ that enter the FRR. We recall the definition

$$A^{\phi}(\boldsymbol{z})=\frac{1}{2\pi(\boldsymbol{z})}\big[N^{\phi}(\boldsymbol{z})\big]^{\mathsf{T}}D(\boldsymbol{z})^{-1}N^{\phi}(\boldsymbol{z}). \tag{A55}$$

For perturbations $\phi\in\{\boldsymbol{F},\ln M,T\}$, using (A20)–(A22), we obtain the following explicit forms of $A^{\phi}(\boldsymbol{z})$:

$$[A^{\boldsymbol{F}}(\boldsymbol{z})]_{kl}=\delta_{kl}\,\frac{\pi(\boldsymbol{z})\mu_k(\boldsymbol{z})}{2T_k(\boldsymbol{z})}, \tag{A56}$$

$$[A^{\ln M}(\boldsymbol{z})]_{kl}=\delta_{kl}\,\frac{\big[j_k^{\rm ss}(\boldsymbol{z})\big]^2}{2\pi(\boldsymbol{z})D_k(\boldsymbol{z})}, \tag{A57}$$

$$[A^{T}(\boldsymbol{z})]_{kl}=\delta_{kl}\,\frac{\mu_k(\boldsymbol{z})\big[\partial_{z_k}\pi(\boldsymbol{z})\big]^2}{2\pi(\boldsymbol{z})T_k(\boldsymbol{z})}. \tag{A58}$$

These expressions are used in Secs. III and V.

Appendix B: Technical details for Markov jump systems

1. Perturbed master equation and local response formulas

In this subsection, we derive the local response formulas stated in Sec. IV. The structure closely parallels Appendix A 1. We consider a local perturbation applied at time $t=0$ on the edge $k \leftrightarrow l$ (with $k>l$). The unperturbed dynamics is governed by

$$\partial_t \boldsymbol{p}(t) = \mathcal{W}\boldsymbol{p}(t), \tag{B1}$$

with stationary distribution $\boldsymbol{\pi}$ satisfying

$$\mathcal{W}\boldsymbol{\pi} = 0. \tag{B2}$$

The evolution under perturbation reads

$$\partial_t \boldsymbol{p}(t) = \big[\mathcal{W} + \epsilon\,\delta(t)\mathcal{K}_{\phi_{kl}}\big]\boldsymbol{p}(t), \tag{B3}$$

where $\phi \in \{F, B\}$ labels the type of perturbation.

An entropic perturbation $F_{kl} \mapsto F_{kl} + \epsilon\delta(t)$ modifies the antisymmetric part of the rates as

$$\delta W_{kl} = \frac{\epsilon}{2} W_{kl}\delta(t), \qquad \delta W_{lk} = -\frac{\epsilon}{2} W_{lk}\delta(t), \tag{B4}$$

which yields

$$\mathcal{K}_{F_{kl}} = \frac{W_{kl}}{2}\big(E_{kl} - E_{ll}\big) - \frac{W_{lk}}{2}\big(E_{lk} - E_{kk}\big). \tag{B5}$$

Likewise, a kinetic perturbation $B_{kl} \mapsto B_{kl} + \epsilon\delta(t)$ modifies the symmetric part of the rates as

$$\delta W_{kl} = \epsilon W_{kl}\delta(t), \qquad \delta W_{lk} = \epsilon W_{lk}\delta(t), \tag{B6}$$

which yields

$$\mathcal{K}_{B_{kl}} = W_{kl}\big(E_{kl} - E_{ll}\big) + W_{lk}\big(E_{lk} - E_{kk}\big). \tag{B7}$$

Here E_{nm} denotes the matrix with a single nonzero entry 1 at row n, column m.

Assuming the steady-state initial condition, we expand

$$\boldsymbol{p}(t) = \boldsymbol{\pi} + \epsilon\,\boldsymbol{q}_{\phi_{kl}}(t) + O(\epsilon^2). \tag{B8}$$

Substituting into the perturbed master equation and retaining only terms linear in ϵ, we obtain

$$\frac{d}{dt}\boldsymbol{q}_{\phi_{kl}}(t) = \mathcal{W}\boldsymbol{q}_{\phi_{kl}}(t) + \delta(t)\mathcal{K}_{\phi_{kl}}\boldsymbol{\pi}, \qquad \boldsymbol{q}_{\phi_{kl}}(0^-) = \boldsymbol{0}. \tag{B9}$$

We define the local prefactor vector by

$$\boldsymbol{N}_{\phi_{kl}} \equiv \mathcal{K}_{\phi_{kl}}\boldsymbol{\pi}. \tag{B10}$$

as a discrete analogue of (27) for Langevin systems. The explicit expressions for $\phi \in \{F, B\}$ follow as

$$\boldsymbol{N}_{F_{kl}} \equiv \mathcal{K}_{F_{kl}}\boldsymbol{\pi} = \frac{a_{kl}}{2}\,(\boldsymbol{e}_k - \boldsymbol{e}_l), \tag{B11}$$

and

$$\boldsymbol{N}_{B_{kl}} \equiv \mathcal{K}_{B_{kl}}\boldsymbol{\pi} = j_{kl}\,(\boldsymbol{e}_k - \boldsymbol{e}_l). \tag{B12}$$

The linearized equation then takes the compact form

$$\frac{d}{dt}\boldsymbol{q}_{\phi_{kl}}(t) = \mathcal{W}\boldsymbol{q}_{\phi_{kl}}(t) + \delta(t)\boldsymbol{N}_{\phi_{kl}}. \tag{B13}$$

Its solution is

$$\boldsymbol{q}_{\phi_{kl}}(t) = e^{\mathcal{W}t}\boldsymbol{N}_{\phi_{kl}} \qquad (t>0). \tag{B14}$$

Since $\langle \eta_n(t)\rangle = p_n(t)$, the response of the empirical state indicator coincides with that of $p_n(t)$ and is given by the nth component of $\boldsymbol{q}_{\phi_{kl}}(t)$. Defining

$$H_{nm}(\omega) = \int_0^\infty \big([e^{\mathcal{W}t}]_{nm} - \pi_n\big)e^{i\omega t}\,dt, \tag{B15}$$

and using the relation $\sum_m (\boldsymbol{N}_{\phi_{kl}})_m = 0$ due to probability conservation, we obtain

$$R^{\eta_n}_{\phi_{kl}}(\omega) = \sum_m H_{nm}(\omega)(\boldsymbol{N}_{\phi_{kl}})_m. \tag{B16}$$

The explicit expressions for $\phi \in \{F, B\}$ follow as

$$R^{\eta_n}_{F_{kl}}(\omega) = \frac{a_{kl}}{2}\big[H_{nk}(\omega) - H_{nl}(\omega)\big], \tag{B17}$$

and

$$R^{\eta_n}_{B_{kl}}(\omega) = j_{kl}\big[H_{nk}(\omega) - H_{nl}(\omega)\big]. \tag{B18}$$

The two responses share a common factor and therefore are proportional to each other:

$$\frac{2}{a_{kl}}R^{\eta_n}_{F_{kl}}(\omega) = \frac{1}{j_{kl}}R^{\eta_n}_{B_{kl}}(\omega) = H_{nk}(\omega) - H_{nl}(\omega). \tag{B19}$$

We next derive the response of the empirical current

$$\jmath_{nm}(t) = \dot{N}_{nm}(t) - \dot{N}_{mn}(t). \tag{B20}$$

For edges different from the perturbed one, the expectation value in the perturbed dynamics is

$$\langle \jmath_{nm}(t)\rangle = W_{nm}p_m(t) - W_{mn}p_n(t), \tag{B21}$$

and therefore the response is entirely determined by the response of $\boldsymbol{p}$. When the observed edge coincides with the perturbed one, there is an additional instantaneous contribution from the explicit perturbation of the rates. Hence the response of the empirical current is given by

$$R^{\jmath_{nm}}_{\phi_{kl}}(\omega) = \Gamma^{\phi}_{nm;kl} + W_{nm}R^{\eta_m}_{\phi_{kl}}(\omega) - W_{mn}R^{\eta_n}_{\phi_{kl}}(\omega), \tag{B22}$$

where

$$\Gamma^{F}_{nm;kl} = \frac{a_{kl}}{2}\big(\delta_{nk}\delta_{ml} - \delta_{nl}\delta_{mk}\big), \tag{B23}$$

and

$$\Gamma^{B}_{nm;kl} = j_{kl}\big(\delta_{nk}\delta_{ml} - \delta_{nl}\delta_{mk}\big). \tag{B24}$$

Substituting (B17) and (B18) into (B22), we obtain

$$R^{\mathcal{J}_{nm}}_{F_{kl}}(\omega) = \frac{a_{kl}}{2}\Big[\delta_{nk}\delta_{ml} - \delta_{nl}\delta_{mk} + W_{nm}\big(H_{mk}(\omega) - H_{ml}(\omega)\big) - W_{mn}\big(H_{nk}(\omega) - H_{nl}(\omega)\big)\Big], \tag{B25}$$

and

$$R^{\mathcal{J}_{nm}}_{B_{kl}}(\omega) = j_{kl}\Big[\delta_{nk}\delta_{ml} - \delta_{nl}\delta_{mk} + W_{nm}\big(H_{mk}(\omega) - H_{ml}(\omega)\big) - W_{mn}\big(H_{nk}(\omega) - H_{nl}(\omega)\big)\Big]. \tag{B26}$$

Equivalently,

$$\frac{2}{a_{kl}} R^{\mathcal{J}_{nm}}_{F_{kl}}(\omega) = \frac{1}{j_{kl}} R^{\mathcal{J}_{nm}}_{B_{kl}}(\omega). \tag{B27}$$

Thus the perturbation type enters only through the amplitudes $a_{kl}/2$ and j_{kl}, while the remaining dynamical dependence is governed by the same excess propagator.

2. Properties of the discrete excess propagator

We now derive several identities for the discrete excess propagator defined in (B15). To this end, we use the following limiting behaviors:

$$\lim_{t\to 0^+} [e^{\mathcal{W}t}]_{nk} = \delta_{nk}, \qquad \lim_{t\to\infty} [e^{\mathcal{W}t}]_{nk} = \pi_n. \tag{B28}$$

First, we show that

$$\sum_m H_{nm}(\omega)\pi_m = 0. \tag{B29}$$

Multiplying (B15) by π_m and summing over m, we obtain

$$\sum_m H_{nm}(\omega)\pi_m = \int_0^\infty dt\, e^{i\omega t} \sum_m \big([e^{\mathcal{W}t}]_{nm} - \pi_n\big)\pi_m = 0. \tag{B30}$$

The last equality follows from stationarity,

$$\sum_m [e^{\mathcal{W}t}]_{nm}\pi_m = \pi_n. \tag{B31}$$

Second, we show that

$$\sum_m \big(i\omega\delta_{nm} + \mathcal{W}_{nm}\big)H_{mk}(\omega) = -\delta_{nk} + \pi_n. \tag{B32}$$

Using

$$\frac{d}{dt}[e^{\mathcal{W}t}]_{nk} = \sum_m \mathcal{W}_{nm}[e^{\mathcal{W}t}]_{mk}, \tag{B33}$$

we obtain

$$\begin{aligned}
&\sum_m \big(i\omega\delta_{nm} + \mathcal{W}_{nm}\big)H_{mk}(\omega)\\
&= \int_0^\infty dt\, e^{i\omega t} \sum_m \Big[i\omega\delta_{nm}\big([e^{\mathcal{W}t}]_{mk} - \pi_m\big) + \mathcal{W}_{nm}[e^{\mathcal{W}t}]_{mk}\Big]\\
&= \int_0^\infty dt\, \partial_t\Big(e^{i\omega t}\big([e^{\mathcal{W}t}]_{nk} - \pi_n\big)\Big)\\
&= -\delta_{nk} + \pi_n.
\end{aligned} \tag{B34}$$

Finally, using

$$\frac{d}{dt}[e^{\mathcal{W}t}]_{nk} = \sum_m [e^{\mathcal{W}t}]_{nm}\mathcal{W}_{mk}, \tag{B35}$$

we analogously obtain

$$\sum_m H_{nm}(\omega)\big(i\omega\delta_{mk} + \mathcal{W}_{mk}\big) = -\delta_{nk} + \pi_n. \tag{B36}$$

Equations (B29)–(B36) show that $H_{nk}(\omega)$ is the resolvent of the Markov generator projected onto the subspace orthogonal to the stationary distribution.

3. Covariances of empirical state indicators and edge currents

We now derive the covariance formulas for the empirical state indicators and empirical edge currents. We begin with

$$\eta_n(t) = \delta_{X(t),n}. \tag{B37}$$

For $t > 0$,

$$\langle \eta_n(t)\eta_m(0)\rangle - \pi_n\pi_m = \big([e^{\mathcal{W}t}]_{nm} - \pi_n\big)\pi_m, \tag{B38}$$

whereas for $t < 0$, by time-translation invariance,

$$\langle \eta_n(t)\eta_m(0)\rangle - \pi_n\pi_m = \big([e^{\mathcal{W}(-t)}]_{mn} - \pi_m\big)\pi_n. \tag{B39}$$

Taking the Fourier transform in time, we obtain

$$C_{\eta_n,\eta_m}(\omega) = H_{nm}(\omega)\pi_m + H_{mn}(-\omega)\pi_n. \tag{B40}$$

As shown in the next subsection, this can be equivalently expressed in the quadratic form

$$C_{\eta_n,\eta_m}(\omega) = \sum_{k>l} a_{kl}\big[H_{nk}(\omega) - H_{nl}(\omega)\big]\big[H_{mk}(-\omega) - H_{ml}(-\omega)\big]. \tag{B41}$$

Next, we decompose the empirical current (54) as

$$\jmath_{nm}(t) = W_{nm}\eta_m(t) - W_{mn}\eta_n(t) + \zeta_{nm}(t), \tag{B42}$$

where we define

$$\zeta_{nm}(t) = [\dot{N}_{nm}(t) - W_{nm}\eta_m(t)] - [\dot{N}_{mn}(t) - W_{mn}\eta_n(t)]\,. \tag{B43}$$

A direct calculation gives

$$\langle \zeta_{nm}(t)\zeta_{kl}(0)\rangle = a_{nm}\big(\delta_{nk}\delta_{ml} - \delta_{nl}\delta_{mk}\big)\delta(t), \tag{B44}$$

and therefore

$$C_{\zeta_{nm},\zeta_{kl}}(\omega) = a_{nm}\big(\delta_{nk}\delta_{ml} - \delta_{nl}\delta_{mk}\big). \tag{B45}$$

We next compute the mixed covariance between the state indicator and the explicit noise part of the current. The definition of $\zeta_{kl}(t)$ and the Markov property yield

$$\langle \eta_n(t)\zeta_{kl}(0)\rangle = a_{kl}\big([e^{\mathcal{W}t}]_{nk} - [e^{\mathcal{W}t}]_{nl}\big), \tag{B46}$$

for $t > 0$, which implies

$$C_{\eta_n,\zeta_{kl}}(\omega) = a_{kl}\big[H_{nk}(\omega) - H_{nl}(\omega)\big]. \tag{B47}$$

Likewise, exchanging the order of the variables and applying $t \to -t$ ($\omega \to -\omega$ in the Fourier domain), we obtain

$$C_{\zeta_{nm},\eta_k}(\omega) = a_{nm}\big[H_{km}(-\omega) - H_{kn}(-\omega)\big]. \tag{B48}$$

From (B42), the mixed state–current covariance reads

$$C_{\eta_n,\jmath_{kl}}(\omega) = W_{kl}C_{\eta_n,\eta_l}(\omega) - W_{lk}C_{\eta_n,\eta_k}(\omega) + C_{\eta_n,\zeta_{kl}}(\omega). \tag{B49}$$

Substituting (B40) and (B47) into (B49), we obtain

$$\begin{aligned} C_{\eta_n,\jmath_{kl}}(\omega) = W_{kl}\Big[H_{nl}(\omega)\pi_l + H_{ln}(-\omega)\pi_n\Big] - W_{lk}\Big[H_{nk}(\omega)\pi_k + H_{kn}(-\omega)\pi_n\Big] \\ + a_{kl}\big[H_{nk}(\omega) - H_{nl}(\omega)\big]. \end{aligned} \tag{B50}$$

Using (B41) and the identity

$$a_{kl}[H_{nk}(\omega) - H_{nl}(\omega)] = \sum_{k'>l'} a_{k'l'}[\delta_{kk'}\delta_{ll'} - \delta_{kl'}\delta_{lk'}][H_{nk'}(\omega) - H_{nl'}(\omega)]\,, \tag{B51}$$

we rewrite (B50) as

$$\begin{aligned} C_{\eta_n,\jmath_{kl}}(\omega) = \sum_{k'>l'} a_{k'l'}[H_{nk'}(\omega) - H_{nl'}(\omega)] \\ \times \{\delta_{kk'}\delta_{ll'} - \delta_{kl'}\delta_{lk'} + W_{kl}[H_{lk'}(-\omega) - H_{ll'}(-\omega)] - W_{lk}[H_{kk'}(-\omega) - H_{kl'}(-\omega)]\} \end{aligned} \tag{B52}$$

Similarly, the current–current covariance reads

$$\begin{aligned} C_{\jmath_{nm},\jmath_{kl}}(\omega) = {} & W_{nm}W_{kl}C_{\eta_m,\eta_l}(\omega) - W_{nm}W_{lk}C_{\eta_m,\eta_k}(\omega) \\ & - W_{mn}W_{kl}C_{\eta_n,\eta_l}(\omega) + W_{mn}W_{lk}C_{\eta_n,\eta_k}(\omega) \\ & + W_{nm}C_{\eta_m,\zeta_{kl}}(\omega) - W_{mn}C_{\eta_n,\zeta_{kl}}(\omega) \\ & + W_{kl}C_{\zeta_{nm},\eta_l}(\omega) - W_{lk}C_{\zeta_{nm},\eta_k}(\omega) + C_{\zeta_{nm},\zeta_{kl}}(\omega). \end{aligned} \tag{B53}$$

Substituting (B41), (B45), and (B47), we obtain

$$\begin{aligned} C_{\jmath_{nm},\jmath_{kl}}(\omega) = \sum_{k'>l'} a_{k'l'}\{\delta_{nk'}\delta_{ml'} - \delta_{nl'}\delta_{mk'} + W_{nm}[H_{mk'}(-\omega) - H_{ml'}(-\omega)] - W_{mn}[H_{nk'}(-\omega) - H_{nl'}(-\omega)]\} \\ \times \{\delta_{kk'}\delta_{ll'} - \delta_{kl'}\delta_{lk'} + W_{kl}[H_{lk'}(-\omega) - H_{ll'}(-\omega)] - W_{lk}[H_{kk'}(-\omega) - H_{kl'}(-\omega)]\}\,. \end{aligned} \tag{B54}$$

4. Proof of the discrete quadratic identity for the state–state covariance

In this subsection, we prove the quadratic representation (B41). To this end, we first rewrite $H_{nm}(\omega)\pi_m$ in terms of a Kronecker-delta function as

$$H_{nm}(\omega)\pi_m = \sum_k H_{nk}(\omega)\pi_k\delta_{km}. \tag{B55}$$

Using the identity (B36) at frequency $-\omega$, we rewrite the Kronecker-delta as

$$\delta_{km} = -\sum_l \big(-i\omega\delta_{lk} + \mathcal{W}_{lk}\big)H_{ml}(-\omega) + \pi_m. \tag{B56}$$

Substituting (B56) into (B55) and using (B29), we have

$$\begin{aligned} H_{nm}(\omega)\pi_m = {} & i\omega \sum_k H_{nk}(\omega)H_{mk}(-\omega)\pi_k \\ & - \sum_{k,l} H_{nk}(\omega)\mathcal{W}_{lk}\pi_k H_{ml}(-\omega). \end{aligned} \tag{B57}$$

Separating the $l=k$ term and using

$$\mathcal{W}_{kk} = -\sum_{l(\neq k)} W_{lk}, \tag{B58}$$

we find

$$\begin{aligned} H_{nm}(\omega)\pi_m = {} & i\omega \sum_k H_{nk}(\omega)H_{mk}(-\omega)\pi_k \\ & + \sum_{k\neq l} H_{nk}(\omega)W_{lk}\pi_k\big[H_{mk}(-\omega) - H_{ml}(-\omega)\big]. \end{aligned} \tag{B59}$$

Similarly, $H_{mn}(-\omega)\pi_n$ is obtained by exchanging $n \leftrightarrow m$ and $\omega \leftrightarrow -\omega$:

$$\begin{aligned} H_{mn}(-\omega)\pi_n = {} & -i\omega \sum_k H_{nk}(\omega)H_{mk}(-\omega)\pi_k \\ & + \sum_{k\neq l} H_{mk}(-\omega)W_{lk}\pi_k\big[H_{nk}(\omega) - H_{nl}(\omega)\big]. \end{aligned} \tag{B60}$$

The state-state covariance is given by the sum of the two expressions (B59) and (B60), where the terms proportional to $i\omega$ cancel.

The resulting expression can be rearranged as

$$C_{\eta_n,\eta_m}(\omega) = \sum_{k\neq l} W_{lk}\pi_k\Big[2H_{nk}(\omega)H_{mk}(-\omega) - H_{nk}(\omega)H_{ml}(-\omega) - H_{nl}(\omega)H_{mk}(-\omega)\Big]. \tag{B61}$$

The stationary condition

$$\sum_{l(\neq k)} W_{lk}\pi_k = \sum_{l(\neq k)} W_{kl}\pi_l. \tag{B62}$$

implies

$$\sum_{k\neq l} W_{lk}\pi_k H_{nk}(\omega)H_{mk}(-\omega) = \sum_{k\neq l} W_{lk}\pi_k H_{nl}(\omega)H_{ml}(-\omega), \tag{B63}$$

under relabelling $k \leftrightarrow l$. Accordingly, (B61) reduces to

$$\begin{aligned} & C_{\eta_n,\eta_m}(\omega) \\ & = \sum_{k\neq l} W_{lk}\pi_k\big[H_{nk}(\omega) - H_{nl}(\omega)\big]\big[H_{mk}(-\omega) - H_{ml}(-\omega)\big]. \end{aligned} \tag{B64}$$

Separating the sum into contributions with $k > l$ and $k < l$, and exchanging dummy indices in the latter, yields (B41).

Appendix C: Derivations of the consequences of the frequency-domain fluctuation–response relation

1. Derivation of the frequency-domain response uncertainty relation

In this subsection, we derive the frequency-domain RUR stated in Sec. V A. This follows directly from the Cauchy–Schwarz inequality applied to the quadratic response representation of the covariance matrix.

We begin with the overdamped Langevin case. For an arbitrary vector $\boldsymbol{u} \in \mathbb{C}^{N_{\rm O}}$, multiplying (42) from the left by $\boldsymbol{u}^\dagger$ and from the right by $\boldsymbol{u}$ gives

$$\begin{aligned} & \boldsymbol{u}^\dagger C_{\boldsymbol{\theta},\boldsymbol{\theta}^\intercal}(\omega)\boldsymbol{u} \\ & = \sum_{k,l=1}^N \int d\boldsymbol{x}\, \boldsymbol{u}^\dagger R^{\boldsymbol{\theta}}_{\phi_k(\boldsymbol{x})}(\omega)\, [A^\phi(\boldsymbol{x})^{-1}]_{kl}\, \big[R^{\boldsymbol{\theta}}_{\phi_l(\boldsymbol{x})}(\omega)\big]^\dagger \boldsymbol{u}. \end{aligned} \tag{C1}$$

We define two functions

$$f_k(\boldsymbol{x},\omega) = \sum_{l=1}^N [A^\phi(\boldsymbol{x})^{1/2}]_{kl}\, \psi_l(\boldsymbol{x},\omega), \tag{C2}$$

and

$$g_k(\boldsymbol{x},\omega;\boldsymbol{u}) = \sum_{l=1}^{N} [A^{\phi}(\boldsymbol{x})^{-1/2}]_{kl} \left[R^{\boldsymbol{\theta}}_{\phi_l(\boldsymbol{x})}(\omega)\right]^{\dagger} \boldsymbol{u}. \tag{C3}$$

that connect the response to a global perturbation $\phi \mapsto \phi + \epsilon\boldsymbol{\psi}$ and the covariance via

$$\sum_{k=1}^{N} \int d\boldsymbol{x}\, g_k(\boldsymbol{x},-\omega;\boldsymbol{u}) f_k(\boldsymbol{x},\omega) = \boldsymbol{u}^{\dagger} R^{\boldsymbol{\theta}}_{\phi\mapsto\phi+\epsilon\boldsymbol{\psi}}(\omega), \tag{C4}$$

and

$$\sum_{k=1}^{N} \int d\boldsymbol{x}\, |g_k(\boldsymbol{x},\omega;\boldsymbol{u})|^2 = \boldsymbol{u}^{\dagger} C_{\boldsymbol{\theta},\boldsymbol{\theta}^{\mathsf{T}}}(\omega) \boldsymbol{u}. \tag{C5}$$

Applying the Cauchy–Schwarz inequality to (C4) yields

$$\begin{aligned} &\left|\boldsymbol{u}^{\dagger} R^{\boldsymbol{\theta}}_{\phi\mapsto\phi+\epsilon\boldsymbol{\psi}}(\omega)\right|^2 \\ &\leq \left[\boldsymbol{u}^{\dagger} C_{\boldsymbol{\theta},\boldsymbol{\theta}^{\mathsf{T}}}(\omega)\boldsymbol{u}\right] \sum_{k,l=1}^{N} \int d\boldsymbol{x}\, \psi_k(\boldsymbol{x},-\omega)\, A^{\phi}_{kl}(\boldsymbol{x})\, \psi_l(\boldsymbol{x},\omega). \end{aligned} \tag{C6}$$

where we used

$$\sum_{k=1}^{N} \int d\boldsymbol{x}\, |f_k(\boldsymbol{x},\omega)|^2 = \sum_{k,l=1}^{N} \int d\boldsymbol{x}\, \psi_k(\boldsymbol{x},-\omega)\, A^{\phi}_{kl}(\boldsymbol{x})\, \psi_l(\boldsymbol{x},\omega). \tag{C7}$$

Assuming that $C_{\boldsymbol{\theta},\boldsymbol{\theta}^{\mathsf{T}}}(\omega)$ is invertible on the subspace considered, we choose

$$\boldsymbol{u} = C_{\boldsymbol{\theta},\boldsymbol{\theta}^{\mathsf{T}}}(\omega)^{-1} R^{\boldsymbol{\theta}}_{\phi\mapsto\phi+\epsilon\boldsymbol{\psi}}(\omega). \tag{C8}$$

This yields

$$\begin{aligned} &\left[R^{\boldsymbol{\theta}}_{\phi\mapsto\phi+\epsilon\boldsymbol{\psi}}(\omega)\right]^{\dagger} C_{\boldsymbol{\theta},\boldsymbol{\theta}^{\mathsf{T}}}(\omega)^{-1} R^{\boldsymbol{\theta}}_{\phi\mapsto\phi+\epsilon\boldsymbol{\psi}}(\omega) \\ &\leq \sum_{k,l=1}^{N} \int d\boldsymbol{x}\, \psi_k(\boldsymbol{x},-\omega)\, A^{\phi}_{kl}(\boldsymbol{x})\, \psi_l(\boldsymbol{x},\omega), \end{aligned} \tag{C9}$$

which establishes the frequency-domain RUR for overdamped Langevin systems.

We next consider Markov jump systems. For an arbitrary vector $\boldsymbol{u} \in \mathbb{C}^{N_O}$, multiplying (84) from the left by $\boldsymbol{u}^{\dagger}$ and from the right by $\boldsymbol{u}$ gives

$$\boldsymbol{u}^{\dagger} C_{\boldsymbol{\theta},\boldsymbol{\theta}^{\mathsf{T}}}(\omega)\boldsymbol{u} = \sum_{n>m} \frac{1}{A^{\phi}_{nm}} \boldsymbol{u}^{\dagger} R^{\boldsymbol{\theta}}_{\phi_{nm}}(\omega) \left[R^{\boldsymbol{\theta}}_{\phi_{nm}}(-\omega)\right]^{\mathsf{T}} \boldsymbol{u}. \tag{C10}$$

We define two objects

$$\begin{aligned} f_{nm}(\omega) &= \sqrt{A^{\phi}_{nm}}\, \psi_{nm}(\omega), \\ g_{nm}(\omega;\boldsymbol{u}) &= \frac{1}{\sqrt{A^{\phi}_{nm}}} R^{\boldsymbol{\theta}}_{\phi_{nm}}(-\omega)^{\mathsf{T}} \boldsymbol{u}, \end{aligned} \tag{C11}$$

that connect the response to a global perturbation $\phi \mapsto \phi + \epsilon\boldsymbol{\psi}$ and the covariance via

$$\sum_{n>m} g_{nm}(\omega;\boldsymbol{u})^* f_{nm}(\omega) = \boldsymbol{u}^{\dagger} R^{\boldsymbol{\theta}}_{\phi\mapsto\phi+\epsilon\boldsymbol{\psi}}(\omega), \tag{C12}$$

and

$$\sum_{n>m} |g_{nm}(\omega;\boldsymbol{u})|^2 = \boldsymbol{u}^{\dagger} C_{\boldsymbol{\theta},\boldsymbol{\theta}^{\mathsf{T}}}(\omega)\boldsymbol{u}. \tag{C13}$$

Applying the Cauchy–Schwarz inequality to (C12) yields

$$\left|\boldsymbol{u}^{\dagger} R^{\boldsymbol{\theta}}_{\phi\mapsto\phi+\epsilon\boldsymbol{\psi}}(\omega)\right|^2 \leq \left[\boldsymbol{u}^{\dagger} C_{\boldsymbol{\theta},\boldsymbol{\theta}^{\mathsf{T}}}(\omega)\boldsymbol{u}\right] \sum_{n>m} A^{\phi}_{nm} |\psi_{nm}(\omega)|^2, \tag{C14}$$

where we used

$$\sum_{n>m} |f_{nm}(\omega)|^2 = \sum_{n>m} A^{\phi}_{nm} |\psi_{nm}(\omega)|^2. \tag{C15}$$

Choosing

$$\boldsymbol{u} = C_{\boldsymbol{\theta},\boldsymbol{\theta}^{\mathsf{T}}}(\omega)^{-1} R^{\boldsymbol{\theta}}_{\phi\mapsto\phi+\epsilon\boldsymbol{\psi}}(\omega), \tag{C16}$$

we arrive at

$$\begin{aligned} &\left[R^{\boldsymbol{\theta}}_{\phi\mapsto\phi+\epsilon\boldsymbol{\psi}}(\omega)\right]^{\dagger} C_{\boldsymbol{\theta},\boldsymbol{\theta}^{\mathsf{T}}}(\omega)^{-1} R^{\boldsymbol{\theta}}_{\phi\mapsto\phi+\epsilon\boldsymbol{\psi}}(\omega) \\ &\leq \sum_{n>m} A^{\phi}_{nm} |\psi_{nm}(\omega)|^2, \end{aligned} \tag{C17}$$

which is the frequency-domain RUR for Markov jump systems.

2. Derivation of the frequency-domain thermodynamic uncertainty relations

In this subsection, we derive the frequency-domain TURs, (97) and (105).

We begin with the overdamped Langevin case. Consider the homogeneous perturbation $\psi_k(\boldsymbol{x},\omega) = 1$ (for all k, $\boldsymbol{x}$, and ω). For a current-like observable

$$\boldsymbol{\theta}(t) = \int d\boldsymbol{x}\, L(\boldsymbol{x}) \boldsymbol{\jmath}(\boldsymbol{x},t), \tag{C18}$$

the corresponding global response is

$$R^{\boldsymbol{\theta}}_{\ln M\mapsto\ln M+\epsilon}(\omega) = \sum_{k=1}^{N} \int d\boldsymbol{z}\, R^{\boldsymbol{\theta}}_{\ln M_k(\boldsymbol{z})}(\omega). \tag{C19}$$

Using (A18), (A19), and (A21), we obtain

$$\begin{aligned}&R^{\boldsymbol{\theta}}_{\ln M\mapsto\ln M+\epsilon}(\omega)\\&=\int d\boldsymbol{x}\,L(\boldsymbol{x})\sum_{k=1}^{N}\int d\boldsymbol{z}\,\mathcal{P}(\boldsymbol{x},\boldsymbol{z};\omega)\,j^{\rm ss}_k(\boldsymbol{z})\,\boldsymbol{e}_k\\&=\int d\boldsymbol{x}\,L(\boldsymbol{x})\left[\boldsymbol{j}_{\rm ss}(\boldsymbol{x})+\hat{\mathcal{J}}_{\boldsymbol{x}}\int d\boldsymbol{z}\,\nabla_{\boldsymbol{z}}^{\sf T}H(\boldsymbol{x},\boldsymbol{z};\omega)\,\boldsymbol{j}_{\rm ss}(\boldsymbol{z})\right].\end{aligned}\tag{C20}$$

The second term vanishes after integration by parts, using the stationarity condition

$$\nabla_{\boldsymbol{z}}^{\sf T}\boldsymbol{j}_{\rm ss}(\boldsymbol{z})=0\tag{C21}$$

and the absence of boundary contributions. Hence, for this choice of perturbation, the response equals the mean value of the current-like observable:

$$R^{\boldsymbol{\theta}}_{\ln M\mapsto\ln M+\epsilon}(\omega)=\int d\boldsymbol{x}\,L(\boldsymbol{x})\boldsymbol{j}_{\rm ss}(\boldsymbol{x})=\langle\boldsymbol{\theta}\rangle_{\rm ss}.\tag{C22}$$

Substituting this into the frequency-domain response TUR (95) yields

$$\langle\boldsymbol{\theta}\rangle_{\rm ss}^{\sf T}C_{\boldsymbol{\theta},\boldsymbol{\theta}^{\sf T}}(\omega)^{-1}\langle\boldsymbol{\theta}\rangle_{\rm ss}\le\frac{\sigma}{2},\tag{C23}$$

which is the frequency-domain TUR for overdamped Langevin systems.

For the Markov jump cases, we consider the homogeneous kinetic perturbation $\psi_{nm}(\omega)=1$ for all $n>m$ and ω. For a single current-like observable $\theta(t)=\sum_{n>m}\Lambda_{nm}\jmath_{nm}(t)$, using (B26), we have

$$\begin{aligned}R^{\theta}_{\boldsymbol{B}\mapsto\boldsymbol{B}}+\epsilon&=\sum_{n>m}\sum_{k>l}\Lambda_{nm}R^{\jmath_{nm}}_{B_{kl}}\\&=\sum_{n>m}\sum_{k>l}\Lambda_{nm}j_{kl}\Big[\delta_{nk}\delta_{ml}-\delta_{nl}\delta_{mk}+W_{nm}\big(H_{mk}(\omega)-H_{ml}(\omega)\big)-W_{mn}\big(H_{nk}(\omega)-H_{nl}(\omega)\big)\Big]\end{aligned}\tag{C24}$$

The terms containing the Kronecker deltas give $\langle\theta\rangle_{\rm ss}$. The remaining terms are of the form $\sum_{k>l}j_{kl}(A_k-A_l)$, with A_k being either $\sum_{n>m}\Lambda_{nm}W_{nm}H_{mk}$ or $\sum_{n>m}\Lambda_{nm}W_{mn}H_{nk}$. They vanish since, for any function A_k of the state,

$$\sum_{k>l}j_{kl}(A_k-A_l)=\sum_k A_k\sum_{l(\neq k)}j_{kl}=0,\tag{C25}$$

where we used the stationarity condition $\sum_{l(\neq k)}j_{kl}=0$. Hence, for this choice of perturbation, the response equals the mean value of the current-like observable: $R^{\theta}_{\boldsymbol{B}\mapsto\boldsymbol{B}+\epsilon}(\omega)=\langle\theta\rangle_{\rm ss}$. This relation extends componentwise to a vector of current-like observables

$$R^{\boldsymbol{\theta}}_{\boldsymbol{B}\mapsto\boldsymbol{B}+\epsilon}(\omega)=\langle\boldsymbol{\theta}\rangle_{\rm ss}.\tag{C26}$$

Substituting this into (104) yields

$$\langle\boldsymbol{\theta}\rangle_{\rm ss}^{\sf T}C_{\boldsymbol{\theta},\boldsymbol{\theta}^{\sf T}}(\omega)^{-1}\langle\boldsymbol{\theta}\rangle_{\rm ss}\le\frac{\sigma^{\rm ps}}{2},\tag{C27}$$

which is the frequency-domain TUR for Markov jump systems.

3. Proof of the equilibrium reciprocity identities

In this subsection, we prove the reciprocity identities used in Sec. V C. We consider the overdamped Langevin and Markov jump cases separately.

We begin with the overdamped Langevin case. At equilibrium, we assume spatially homogeneous temperature $T_k(\boldsymbol{x})=T$ and conservative force $F_k(\boldsymbol{x})=-\partial_{x_k}U(\boldsymbol{x})$, so that the steady state is given by $\pi(\boldsymbol{x})\propto e^{-U(\boldsymbol{x})/T}$. Time-reversal symmetry then implies detailed balance for the propagator,

$$P(\boldsymbol{x},t|\boldsymbol{z},0)\pi(\boldsymbol{z})=P(\boldsymbol{z},t|\boldsymbol{x},0)\pi(\boldsymbol{x}).\tag{C28}$$

Integrating this relation over $t\in[0,\infty)$ with the factor $e^{i\omega t}$, we obtain

$$H(\boldsymbol{x},\boldsymbol{z};\omega)\pi(\boldsymbol{z})=H(\boldsymbol{z},\boldsymbol{x};\omega)\pi(\boldsymbol{x}).\tag{C29}$$

We consider the local current response to a force perturbation. Using (A18)–(A20), we obtain the ij component of the response function:

$$\begin{aligned}&\big[R^{\boldsymbol{\jmath}(\boldsymbol{x})}_{\boldsymbol{F}(\boldsymbol{z})}(\omega)\big]_{ij}=\mu_i(\boldsymbol{x})\pi(\boldsymbol{x})\delta_{ij}\delta(\boldsymbol{x}-\boldsymbol{z})\\&+\mu_i(\boldsymbol{x})\mu_j(\boldsymbol{z})\big[F_i(\boldsymbol{x})-T\partial_{x_i}\big]\partial_{z_j}H(\boldsymbol{x},\boldsymbol{z};\omega)\,\pi(\boldsymbol{z}).\end{aligned}\tag{C30}$$

Using (C29) and

$$\big[F_i(\boldsymbol{x})-T\partial_{x_i}\big]\pi(\boldsymbol{x})=0,\tag{C31}$$

the second term becomes

$$-\mu_i(\boldsymbol{x})\mu_j(\boldsymbol{z})T\pi(\boldsymbol{x})\,\partial_{x_i}\partial_{z_j}H(\boldsymbol{z},\boldsymbol{x};\omega).\tag{C32}$$

The same expression is obtained upon exchanging $(i,\boldsymbol{x})\leftrightarrow(j,\boldsymbol{z})$. Therefore, the response function (C30) satisfies the reciprocity identity:

$$\left[R^{\mathcal{J}(\boldsymbol{x})}_{\boldsymbol{F}(\boldsymbol{z})}(\omega)\right]_{ij} = \left[R^{\mathcal{J}(\boldsymbol{z})}_{\boldsymbol{F}(\boldsymbol{x})}(\omega)\right]_{ji}. \tag{C33}$$

and, in matrix form,

$$\left[R^{\mathcal{J}(\boldsymbol{x})}_{\boldsymbol{F}(\boldsymbol{z})}(\omega)\right]_{\rm eq} = \left[R^{\mathcal{J}(\boldsymbol{z})}_{\boldsymbol{F}(\boldsymbol{x})}(\omega)\right]^{\mathsf{T}}_{\rm eq}. \tag{C34}$$

We now turn to Markov jump systems and prove the discrete reciprocity relation

$$\left[R^{\mathcal{J}_{nm}}_{F_{kl}}(\omega)\right]_{\rm eq} = \left[R^{\mathcal{J}_{kl}}_{F_{nm}}(\omega)\right]_{\rm eq}. \tag{C35}$$

For clarity, we proceed in the time domain. The time-domain counterpart of the response function (B25) reads

$$r^{\mathcal{J}_{nm}}_{F_{kl}}(t) = \frac{a_{kl}}{2}\Big[\big(\delta_{nk}\delta_{ml} - \delta_{nl}\delta_{mk}\big)\delta(t) + W_{nm}\big(P_{mk}(t) - P_{ml}(t)\big) - W_{mn}\big(P_{nk}(t) - P_{nl}(t)\big)\Big], \tag{C36}$$

where $P_{ab}(t) \equiv [e^{\mathcal{W}t}]_{ab}$.

At equilibrium, detailed balance implies

$$W_{ab}\pi_b = W_{ba}\pi_a, \qquad \pi_b P_{ab}(t) = \pi_a P_{ba}(t), \tag{C37}$$

which in turn yields

$$a_{ab} = 2W_{ab}\pi_b = 2W_{ba}\pi_a. \tag{C38}$$

To prove the reciprocity (C35), we examine how the terms in the response function (C36) transform under the exchange $(nm) \leftrightarrow (kl)$ at equilibrium. The singular term proportional to $\delta(t)$ is manifestly symmetric. For the regular part, the individual terms are not separately invariant, but are mapped into one another. We next examine one of the regular terms $(a_{kl}/2)W_{nm}P_{mk}(t)$. By repeated use of the detailed balance conditions (C37) and (C38), we obtain

$$\begin{aligned}\frac{a_{kl}}{2}W_{nm}P_{mk}(t) &= W_{kl}\pi_l W_{nm}P_{mk}(t)\\ &= W_{mn}\pi_n W_{lk}P_{km}(t)\\ &= \frac{a_{nm}}{2}W_{lk}P_{km}(t).\end{aligned} \tag{C39}$$

This reflects the balance between the trajectory $(l \to k \to \cdots \to m \to n)$ and its time reversal $(n \to m \to \cdots \to k \to l)$. The remaining three regular terms are handled in the same way:

$$\frac{a_{kl}}{2}W_{nm}P_{ml}(t) = \frac{a_{nm}}{2}W_{kl}P_{lm}(t), \tag{C40}$$

$$\frac{a_{kl}}{2}W_{mn}P_{nk}(t) = \frac{a_{nm}}{2}W_{lk}P_{kn}(t), \tag{C41}$$

and

$$\frac{a_{kl}}{2}W_{mn}P_{nl}(t) = \frac{a_{nm}}{2}W_{kl}P_{ln}(t). \tag{C42}$$

Taken (C39)–(C42) together, the regular part of the response function (C36) is as a whole symmetric under $(nm) \leftrightarrow (kl)$. Thus, the full time-domain response (C36) is symmetric under the exchange $(nm) \leftrightarrow (kl)$,

$$r^{\mathcal{J}_{nm}}_{F_{kl}}(t) = r^{\mathcal{J}_{kl}}_{F_{nm}}(t) \qquad (t \geq 0). \tag{C43}$$

Taking the Fourier transform, we obtain

$$\left[R^{\mathcal{J}_{nm}}_{F_{kl}}(\omega)\right]_{\rm eq} = \left[R^{\mathcal{J}_{kl}}_{F_{nm}}(\omega)\right]_{\rm eq}, \tag{C44}$$

which is the reciprocity identity used in Sec. V C.

4. Alternative covariance–response identities

In this subsection, we derive the alternative covariance–response identities (108) and (111) used in Secs. V C and V D.

For overdamped Langevin systems, (A18) and (A20) yield the force-response formula

$$R^{\mathcal{J}(\boldsymbol{x})}_{\boldsymbol{F}(\boldsymbol{y})}(\omega) = \mathcal{P}(\boldsymbol{x},\boldsymbol{y};\omega)M(\boldsymbol{y})\pi(\boldsymbol{y}). \tag{C45}$$

Recalling the relation $D(\boldsymbol{y}) = M(\boldsymbol{y})T(\boldsymbol{y})$, we can rewrite the current-current covariance (A49) as:

$$\begin{aligned}C_{\mathcal{J}(\boldsymbol{x}),\mathcal{J}(\boldsymbol{y})^{\mathsf{T}}}(\omega) &= \int d\boldsymbol{z}\; R^{\mathcal{J}(\boldsymbol{x})}_{\boldsymbol{F}(\boldsymbol{z})}(\omega)T(\boldsymbol{z})\big[\mathcal{P}(\boldsymbol{y},\boldsymbol{z};\omega)\big]^{\dagger} + \int d\boldsymbol{z}\; \mathcal{P}(\boldsymbol{x},\boldsymbol{z};\omega)\big[R^{\mathcal{J}(\boldsymbol{y})}_{\boldsymbol{F}(\boldsymbol{z})}(\omega)T(\boldsymbol{z})\big]^{\dagger}\\ &= R^{\mathcal{J}(\boldsymbol{x})}_{\boldsymbol{F}(\boldsymbol{y})}(\omega)\,T(\boldsymbol{y}) + T(\boldsymbol{x})\big[R^{\mathcal{J}(\boldsymbol{y})}_{\boldsymbol{F}(\boldsymbol{x})}(\omega)\big]^{\dagger}\\ &\quad + \int d\boldsymbol{z}\; R^{\mathcal{J}(\boldsymbol{x})}_{\boldsymbol{F}(\boldsymbol{z})}(\omega)T(\boldsymbol{z})\big[\hat{\mathcal{J}}_{\boldsymbol{y}}\boldsymbol{\nabla}^{\mathsf{T}}_{\boldsymbol{z}}H(\boldsymbol{y},\boldsymbol{z};\omega)\big]^{\dagger} + \int d\boldsymbol{z}\; \hat{\mathcal{J}}_{\boldsymbol{x}}\boldsymbol{\nabla}^{\mathsf{T}}_{\boldsymbol{z}}H(\boldsymbol{x},\boldsymbol{z};\omega)T(\boldsymbol{z})\big[R^{\mathcal{J}(\boldsymbol{y})}_{\boldsymbol{F}(\boldsymbol{z})}(\omega)\big]^{\dagger}\end{aligned} \tag{C46}$$

Using the equivalence between the two expression (A37) and (A38) reduces the integral terms to

$$\hat{\mathcal{J}}_{\boldsymbol{x}}\Big(\pi(\boldsymbol{y})D(\boldsymbol{y})\boldsymbol{\nabla}_{\boldsymbol{y}}^{\mathsf{T}}H(\boldsymbol{x},\boldsymbol{y};\omega)+\hat{\mathcal{J}}_{\boldsymbol{y}}^{\mathsf{T}}\big[\pi(\boldsymbol{y})H(\boldsymbol{x},\boldsymbol{y};\omega)\big]\Big)+\Big[\hat{\mathcal{J}}_{\boldsymbol{y}}\Big(\pi(\boldsymbol{x})D(\boldsymbol{x})\boldsymbol{\nabla}_{\boldsymbol{x}}^{\mathsf{T}}H(\boldsymbol{y},\boldsymbol{x};-\omega)+\hat{\mathcal{J}}_{\boldsymbol{x}}^{\mathsf{T}}\big[\pi(\boldsymbol{x})H(\boldsymbol{y},\boldsymbol{x};-\omega)\big]\Big)\Big]^{\mathsf{T}}$$
$$=\big[\hat{\mathcal{J}}_{\boldsymbol{x}}H(\boldsymbol{x},\boldsymbol{y};\omega)\big]\boldsymbol{j}_{\mathrm{ss}}(\boldsymbol{y})^{\mathsf{T}}+\boldsymbol{j}_{\mathrm{ss}}(\boldsymbol{x})\big[\hat{\mathcal{J}}_{\boldsymbol{y}}H(\boldsymbol{y},\boldsymbol{x};-\omega)\big]^{\mathsf{T}}, \tag{C47}$$

where $\hat{\mathcal{J}}_{\bullet}^{\mathsf{T}}$ ($\bullet\in\{\boldsymbol{x},\boldsymbol{y}\}$) operators in the first line act on the entire bracketed expression. Replacing the integral terms in (C46) with (C47), we obtain alternative covariance–response identity

$$C_{\boldsymbol{\jmath}(\boldsymbol{x}),\boldsymbol{\jmath}(\boldsymbol{y})^{\mathsf{T}}}(\omega)=R^{\boldsymbol{\jmath}(\boldsymbol{x})}_{\boldsymbol{F}(\boldsymbol{y})}(\omega)\,T(\boldsymbol{y})+T(\boldsymbol{x})\big[R^{\boldsymbol{\jmath}(\boldsymbol{y})}_{\boldsymbol{F}(\boldsymbol{x})}(\omega)\big]^{\dagger}+\big[\hat{\mathcal{J}}_{\boldsymbol{x}}H(\boldsymbol{x},\boldsymbol{y};\omega)\big]\boldsymbol{j}_{\mathrm{ss}}(\boldsymbol{y})^{\mathsf{T}}+\boldsymbol{j}_{\mathrm{ss}}(\boldsymbol{x})\big[\hat{\mathcal{J}}_{\boldsymbol{y}}H(\boldsymbol{y},\boldsymbol{x};-\omega)\big]^{\mathsf{T}}. \tag{C48}$$

We next turn to the Markov jump system. Substituting (B41), (B45), (B47), and (B48) into (B53), the current-current covariance $C_{\jmath_{nm},\jmath_{n'm'}}$ can be decomposed as three contributions: (i) ω-independent term $C_{\zeta_{nm},\zeta_{n'm'}}=a_{nm}(\delta_{nn'}\delta_{mm'}-\delta_{nm'}\delta_{mn'})$, (ii) the terms involving $H(\omega)$, and (iii) the terms involving $H(-\omega)$. The terms involving $H(\omega)$ are collected as

$$W_{n'm'}\pi_{m'}\big[W_{nm}H_{mn'}(\omega)-W_{mn}H_{nn'}(\omega)\big]-W_{m'n'}\pi_{n'}\big[W_{nm}H_{mm'}(\omega)-W_{mn}H_{nm'}(\omega)\big] \tag{C49}$$

Using $W_{n'm'}\pi_{m'}=(a_{n'm'}+j_{n'm'})/2$ and $W_{m'n'}\pi_{n'}=(a_{n'm'}-j_{n'm'})/2$, this is decomposed into

$$\begin{aligned}&\frac{a_{n'm'}}{2}\Big(W_{nm}\big[H_{mn'}(\omega)-H_{mm'}(\omega)\big]-W_{mn}\big[H_{nn'}(\omega)-H_{nm'}(\omega)\big]\Big)\\&+\frac{j_{n'm'}}{2}\Big(W_{nm}\big[H_{mn'}(\omega)+H_{mm'}(\omega)\big]-W_{mn}\big[H_{nn'}(\omega)+H_{nm'}(\omega)\big]\Big)\end{aligned} \tag{C50}$$

Together with the half of ω-independent term $C_{\zeta_{nm},\zeta_{n'm'}}$, the first line of (C50) matches $R^{\jmath_{nm}}_{F_{n'm'}}(\omega)$ in (B25). For convenience, we define

$$Z_{nm,n'm'}(\omega)\equiv\frac{1}{2}W_{nm}\big[H_{mn'}(\omega)+H_{mm'}(\omega)\big]j_{n'm'} \tag{C51}$$

so that the second line of (C50) is briefly expressed as $Z_{nm,n'm'}(\omega)-Z_{mn,n'm'}(\omega)$.

The terms involving $H(-\omega)$ are given by the same expression with exchanging $(n,m,\omega)\leftrightarrow(n',m',-\omega)$

$$C_{\jmath_{nm},\jmath_{n'm'}}(\omega)=R^{\jmath_{nm}}_{F_{n'm'}}(\omega)+R^{\jmath_{n'm'}}_{F_{nm}}(-\omega)+Z_{nm,n'm'}(\omega)-Z_{mn,n'm'}(\omega)+Z_{n'm',nm}(-\omega)-Z_{m'n',nm}(-\omega).\quad . \tag{C52}$$

We denote the current-dependent contributions by

$$\Delta_{nm,n'm'}(\omega)\equiv Z_{nm,n'm'}(\omega)-Z_{mn,n'm'}(\omega)+Z_{n'm',nm}(-\omega)-Z_{m'n',nm}(-\omega), \tag{C53}$$

so that

$$C_{\jmath_{nm},\jmath_{n'm'}}(\omega)=R^{\jmath_{nm}}_{F_{n'm'}}(\omega)+R^{\jmath_{n'm'}}_{F_{nm}}(-\omega)+\Delta_{nm,n'm'}(\omega). \tag{C54}$$

[1] R. Kubo, Reports on Progress in Physics **29**, 255 (1966).
[2] G. S. Agarwal, Zeitschrift für Physik A Hadrons and nuclei **252**, 25 (1972).
[3] T. Speck and U. Seifert, Europhysics Letters **74**, 391 (2006).
[4] M. Baiesi, C. Maes, and B. Wynants, Phys. Rev. Lett. **103**, 010602 (2009).
[5] J. Prost, J.-F. Joanny, and J. M. R. Parrondo, Phys. Rev. Lett. **103**, 090601 (2009).
[6] U. Seifert and T. Speck, Europhysics Letters **89**, 10007 (2010).
[7] B. Altaner, M. Polettini, and M. Esposito, Phys. Rev. Lett. **117**, 180601 (2016).
[8] T. Harada and S.-i. Sasa, Phys. Rev. Lett. **95**, 130602 (2005).
[9] T. Harada and S.-i. Sasa, Phys. Rev. E **73**, 026131 (2006).
[10] R. Golestanian, Phys. Rev. Lett. **134**, 207101 (2025).
[11] A. C. Barato and U. Seifert, Phys. Rev. Lett. **114**, 158101 (2015).
[12] T. R. Gingrich, J. M. Horowitz, N. Perunov, and J. L. England, Phys. Rev. Lett. **116**, 120601 (2016).
[13] P. Pietzonka, A. C. Barato, and U. Seifert, Phys. Rev. E

93, 052145 (2016).
[14] P. Pietzonka, F. Ritort, and U. Seifert, Phys. Rev. E **96**, 012101 (2017).
[15] J. M. Horowitz and T. R. Gingrich, Phys. Rev. E **96**, 020103 (2017).
[16] I. Di Terlizzi and M. Baiesi, Journal of Physics A: Mathematical and Theoretical **52**, 02LT03 (2018).
[17] G. Falasco, M. Esposito, and J.-C. Delvenne, New Journal of Physics **22**, 053046 (2020).
[18] J. M. Horowitz and T. R. Gingrich, Nature Physics **16**, 15 (2020).
[19] J. S. Lee, J.-M. Park, and H. Park, Phys. Rev. E **104**, L052102 (2021).
[20] V. T. Vo, T. Van Vu, and Y. Hasegawa, Journal of Physics A: Mathematical and Theoretical **55**, 405004 (2022).
[21] E. Kwon, J.-M. Park, J. S. Lee, and Y. Baek, Phys. Rev. E **110**, 044131 (2024).
[22] A. Dechant and S. ichi Sasa, Proceedings of the National Academy of Sciences **117**, 6430 (2020), https://www.pnas.org/doi/pdf/10.1073/pnas.1918386117.
[23] Q. Gao, H.-M. Chun, and J. M. Horowitz, Phys. Rev. E **105**, L012102 (2022).
[24] H.-M. Chun and J. M. Horowitz, The Journal of Chemical Physics **158**, 174115 (2023).
[25] G. Fernandes Martins and J. M. Horowitz, Phys. Rev. E **108**, 044113 (2023).
[26] T. Aslyamov and M. Esposito, Phys. Rev. Lett. **132**, 037101 (2024).
[27] Q. Gao, H.-M. Chun, and J. M. Horowitz, Europhysics Letters **146**, 31001 (2024).
[28] K. Ptaszyński, T. Aslyamov, and M. Esposito, Phys. Rev. Lett. **133**, 227101 (2024).
[29] K. Liu and J. Gu, Communications Physics **8**, 62 (2025).
[30] T. Aslyamov, K. Ptaszyński, and M. Esposito, Phys. Rev. Lett. **134**, 157101 (2025).
[31] K. Ptaszyński, T. Aslyamov, and M. Esposito, Phys. Rev. E **113**, 024130 (2026).
[32] K. Ptaszyński, T. Aslyamov, and M. Esposito, Phys. Rev. E **113**, 024131 (2026).
[33] E. Kwon, H.-M. Chun, H. Park, and J. S. Lee, Phys. Rev. Lett. **135**, 097101 (2025).
[34] H.-M. Chun, E. Kwon, H. Park, and J. S. Lee, Fluctuation-response theory for nonequilibrium langevin dynamics (2026), arXiv:2601.16387 [cond-mat.stat-mech].
[35] A. Dechant, Finite-frequency fluctuation-response inequality (2025), arXiv:2510.15228 [cond-mat.stat-mech].
[36] T. Aslyamov, K. Ptaszyński, and M. Esposito, Phys. Rev. Lett. **136**, 067102 (2026).
[37] T. Aslyamov and M. Esposito, Dynamical fluctuation-response relations (2026), arXiv:2604.24626 [cond-mat.stat-mech].
[38] T. Aslyamov and M. Esposito, arXiv preprint arXiv:2507.07876 (2025).
[39] C. Maes and K. Netočný, EPL (Europhysics Letters) **82**, 30003 (2008).
[40] J. Keizer, *Statistical thermodynamics of nonequilibrium processes* (Springer Science & Business Media, 2012).
[41] A. Dechant, Journal of Physics A: Mathematical and Theoretical **52**, 035001 (2018).
[42] C. Maes, Physics Reports **850**, 1 (2020).
[43] J. Schnakenberg, Reviews of Modern physics **48**, 571 (1976).
[44] T. Hill, *Free energy transduction in biology: the steady-state kinetic and thermodynamic formalism* (Elsevier, 2012).
[45] M. Polettini, G. Bulnes-Cuetara, and M. Esposito, Physical Review E **94**, 052117 (2016).
[46] F. Avanzini, M. Bilancioni, V. Cavina, S. Dal Cengio, M. Esposito, G. Falasco, D. Forastiere, J. N. Freitas, A. Garilli, P. E. Harunari, *et al.*, SciPost Physics Lecture Notes , 080 (2024).
[47] H. Vroylandt, D. Lacoste, and G. Verley, Journal of Statistical Mechanics: Theory and Experiment **2018**, 023205 (2018).
[48] H. Vroylandt, D. Lacoste, and G. Verley, Journal of Statistical Mechanics: Theory and Experiment **2019**, 054002 (2019).
[49] J. S. van Zon, D. K. Lubensky, P. R. Altena, and P. R. ten Wolde, Proceedings of the National Academy of Sciences **104**, 7420 (2007).
[50] A. C. Barato and U. Seifert, Physical Review E **95**, 062409 (2017).
[51] H. Risken, in *The Fokker-Planck equation: methods of solution and applications* (Springer, 1989) pp. 63–95.
[52] P. Reimann, C. Van den Broeck, H. Linke, P. Hänggi, J. M. Rubi, and A. Pérez-Madrid, Phys. Rev. Lett. **87**, 010602 (2001).
[53] P. Reimann, C. Van den Broeck, H. Linke, P. Hänggi, J. M. Rubi, and A. Pérez-Madrid, Phys. Rev. E **65**, 031104 (2002).
[54] R. Hayashi, K. Sasaki, S. Nakamura, S. Kudo, Y. Inoue, H. Noji, and K. Hayashi, Phys. Rev. Lett. **114**, 248101 (2015).
[55] A. Dechant and S.-i. Sasa, Physical Review E **97**, 062101 (2018).